







Article

Influence of Injection Pressure and Aluminium Oxide Nano Particle-Added Fish Oil Methyl Ester on the Performance and Emission of Compression Ignition Engine

K. M. Akkoli ^{1,*}, S. C. Kamate ¹, S. N. Topannavar ¹, A. R. Bhavimani ¹, N. R. Banapurmath ², Ibham Veza ³, Manzoore Elahi M. Soudagar ^{4,*}, T. M. Yunus Khan ⁵, A. S. El-Shafay ⁶, M. A. Kalam ⁷, M. M. Shivashimpi ¹ and Archana M. Gulli ¹

¹ Mechanical Engineering Department, Hirasugar Institute of Technology, Nidasoshi 591236, Karnataka, India

² Department of Mechanical Engineering, B.V.B. College of Engineering and Technology, Hubli 580031, Karnataka, India

³ Department of Mechanical Engineering, Universiti Teknologi PETRONAS, Bandar Seri Iskandar 32610, Perak Darul Ridzuan, Malaysia

⁴ Department of Mechanical Engineering, Faculty of Mechanical Engineering, University of Malaya, Kuala Lumpur 50603, Malaysia

⁵ Department of Mechanical Engineering, College of Engineering, King Khalid University, Abha 61421, Saudi Arabia

⁶ Department of Mechanical Engineering, College of Engineering, Prince Sattam bin Abdulaziz University, Alkharj 16273, Saudi Arabia

⁷ School of Civil and Environmental Engineering, FEIT, University of Technology Sydney, Sydney, NSW 2007, Australia

* Correspondence: km_akkoli@yahoo.co.in (K.M.A.); me.soudagar@gmail.com (M.E.M.S.)



Citation: Akkoli, K.M.; Kamate, S.C.; Topannavar, S.N.; Bhavimani, A.R.; Banapurmath, N.R.; Veza, I;

Soudagar, M.E.M.; Khan, T.M.Y.; El-Shafay, A.S.; Kalam, M.A.; et al. Influence of Injection Pressure and Aluminium Oxide Nano Particle-Added Fish Oil Methyl Ester on the Performance and Emission of Compression Ignition Engine.

Energies **2022**, *15*, 9491. <https://doi.org/10.3390/en15249491>

Academic Editor: Constantine D. Rakopoulos

Received: 5 November 2022

Accepted: 6 December 2022

Published: 14 December 2022

Publisher's Note: MDPI stays neutral with regard to jurisdictional claims in published maps and institutional affiliations.



Copyright: © 2022 by the authors. Licensee MDPI, Basel, Switzerland. This article is an open access article distributed under the terms and conditions of the Creative Commons Attribution (CC BY) license (<https://creativecommons.org/licenses/by/4.0/>).

Abstract: The present experimental examination was carried out to suggest a better fuel blend with an optimised dosage level of alumina nanoparticles (Al_2O_3)—in a mixture of Fish Oil Methyl Ester (FOME) biodiesel and diesel—and injection pressure, wherein enhanced performance and reduced emissions were obtained via a diesel engine. The aluminium nanoparticles were added to the mixture in 5 mg/l steps through varying concentrations from 5 to 20 mg/L. The experimental results showed that engine performance quietly reduces with increased emission characteristics with the addition of raw FOME biodiesel compared to diesel. Furthermore, the addition of aluminium nanoparticles (Al_2O_3) improved the performance as well as the emission characteristics of the engine. Among all the test blends, the B40D60A20 blend provided a maximum brake thermal efficiency of 30.7%, which is 15.63% superior to raw FOME and 3.90% inferior to diesel fuel. The blend also showed reduced emissions, for instance, a reduction of 48.38% in CO, 17.51% in HC, 16.52% in NO_x, and 20.89% in smoke compared to diesel fuel. Lastly, it was concluded that B40D60A20 at 260 bar is the optimised fuel blend, and 20 mg/l is the recommended dose level of aluminium nanoparticles (Al_2O_3) in the FOME–diesel mixture biodiesels in order to enhance the performance and emission parameters of a diesel engine.

Keywords: aluminium nanoparticles; fish biodiesel; common rail direct injection; emission and performance

1. Introduction

Nowadays, there is a greater requirement for diesel, on average, compared to the other fuels. Diesel engines play an extensive role in the transportation sector, trains, industries, and the irrigation sector [1,2]. Compression-ignition engines are generally more efficient than spark ignition engines. However, the price of conventional fuels is gradually increasing. Diesel engines are the source of numerous poisonous emissions, such as particulate matter and nitrogen oxides, that cause acid rain formation, ozone

layer depletion, the production of greenhouse gases, smog formation, and unwanted climatic changes [3,4]. Diesel engine emissions can be reduced through various approaches, including the modification of the engine's design, the enhancement of engine combustion, the treatment of exhaust, and the use of fuel additives to reduce diesel emissions [5–7]. The use of oxygenated fuels such as biodiesel is the best choice as a substitute for conventional diesel fuel. The major challenges that cannot be met by diesel today can be overcome using biodiesel. Thus, the emissions of diesel engines can be considerably reduced by using biodiesels in diesel engines [8,9].

The transesterification process is used to extract biodiesel from various plants, both edible and non-edible; chicken fat; tallow oil of beef; waste cooking oils; and pork lard. The use of biodiesel over diesel fuel minimises the high flashpoint, high lubricity, high cetane number non-toxicity, and content of sulphur and aromatic hydrocarbons in the fuel. Non-edible biodiesels are the most preferred with respect to overcoming the further food requirement-related problems around the world. The commonly suggested non-edible oils are produced from plants that can be cultivated on land that is barren utilizing wastewater or that can be produced from a plant that does not require a considerable amount of water. The production of such non-edible biofuels will help countries reduce their importation of fossil fuels from other countries; alternatively, it serves as a backup until the current fuel reserves are depleted [10–12]. Fish oil is an oil extracted from fish fat and is known to be a promising source for biodiesel that functions as a backup for diesel. For the present study, fish oil methyl ester, which is obtained by the transesterification process using methanol with potassium hydroxide as a catalyst, was used.

Biodiesel is considered today's best alternative to diesel fuel. To enhance the performance and reduce emissions, a great deal of experimental investigation is being undertaken with respect to the addition of nano additives. So far, the experimental results have demonstrated that metal oxides such as Cerium Oxide (CeO), Carbon Nanotubes (CNT), Alumina (Al₂O₃), Manganese Oxide (MnO), Copper Oxide (CuO), and Zinc Oxide (ZnO) can be extensively used as fuel additives in the mixture of biodiesel and diesel. These nanoparticles are very small, ranging from 1 to 100 nm. The nanoparticles provide a large surface area for combustion and hence act as a catalyst [13]. Thus, the emission of exhaust gases formed due to the incomplete burning of fuel is reduced and combustion efficiency increases. The consumption of fuel and the emission of gases from diesel engines can be influenced by the size and chemical composition of the nanoparticles along with the optimised mixture of the fraction of biodiesel and diesel fuel.

Attia A. M. et al. [14] studied alumina nanoparticle additives' effects on a mixture of 20% jojoba biodiesel and 80% diesel. The amount of alumina nanoparticles in the mixture varied from 10 to 50 mg/l. The addition of nano additives showed a reduction in the overall BSFC by about 6% and a 7% enhancement in the engine thermal efficiency. In addition, it was observed that NO_x and CO emissions were reduced by 70% and 75%, and smoke opacity and UHC were reduced by 5% and 55%, respectively. The fuel blend of 30 mg/L with 20% biodiesel provided optimised engine performance. Ahmed EL-Seesy et al. [15] analysed CI engines' emissions with performance fuelled by diesel, nanoparticles, and Jojoba biodiesel. Nanoparticles with a 10 to 15 nm diameter and 1–10 microns in length were used at a dosage level of 10 to 50 mg/L blended with diesel. The nano-dose level of 50 mg/L provided superior mechanical performance and the dosage of 20 mg/L provided remarkable ecological performance. Lastly, they concluded that a dosage of 40 mg/L is recommended for the enhanced performance of the engine. Arul Mozhi Selvan.V. et al. [16] used cerium oxide nanoparticles to examine the effects on the performance and emission parameters of CI engines operating with pure diesel and diesel biodiesel–ethanol blends. They observed that the fuel mixture of 70% diesel and 10% biodiesel + 20% ethanol + 25 ppm CeO₃ enhanced the ignition delay and brakes' thermal efficiency with reduced emissions of CO, HC, NO, and smoke. Jeryraj Kumar et al. [17] demonstrated the influence of a nanoparticle, Calophyllum innophyllum biodiesel, and diesel fuel mixture on the exhaust emissions and performance (BTE/BSFC) of CI engines. The results showed that

enhanced brake thermal efficiency and high NO_x emission reduced emissions after the fuels were blended with nanoparticles. Karthikeyan. S. et al. [18] examined aluminium oxide nanoparticles' effect on the emission and performance parameters of a CI engine operated with a mixture of diesel and methyl esters of grape seed oil Biodiesel (GSOME). The test fuel used for the study was D80B20Al₂O₃50 ppm and D80B20Al₂O₃100 ppm. From the results, they concluded that the D80B20Al₂O₃50 ppm blend showed the best performance and emission characteristics with an optimised dose level of 50 ppm Al₂O₃. Jayanthi. P et al. [19] investigated copper oxide nanoparticles' effects on a DI engine's emission and performance characteristics. The nanoparticles were blended with biodiesel at dosage levels of 40, 80, and 120 ppm using an ultra-sonicator. Lastly, from the results, they concluded that the fuel blend B20+ 80 ppm reduces HC, CO, smoke, and NO_x emissions and enhances the BTE with a decrease in SFC at all load conditions. Jothi Thirumal. B. et al. [20] investigated cerium oxide's influence on the performance and emissions of diesel engines. They used fuel blends of diesel + CeO 25 ppm and diesel + CeO 50 ppm for the study. Lastly, from the results, they concluded that the fuel blend CeO 50 ppm showed a 6% greater improvement in BTE than diesel, and emissions of CO were reduced by 35.65%, those of NO_x by 62.7%, smoke by 15%, and HC by 56.5%. Kasireddy Sravani. et al [21] used a mixture of Pongamia Biodiesel, diesel, and oxides of Zinc particles as nano-additives in different ppm proportions—B20, B20 + 80, B20 + 120, and B20 + 40—in an IC engine to analyse zinc oxide nanoparticles' influence on the emissions and performance characteristics of the engine. They observed that the B20 + 80 ppm blend showed superior brake thermal efficiency and minimised emissions when compared with diesel. Karthikeyan.S. et al. [22] analysed the performance and emission characteristics of CI engines fuelled by canola oil methyl ester and zinc oxide nano-additives. The fuel dose levels used were D80B20, D80B20ZnO50 ppm, and D80B20ZnO100 ppm prepared using an ultra-sonicator. In their results, they concluded that the D80B20ZnO50 ppm blend showed the best performance and emission characteristics with an optimised dose level of 50 ppm ZnO. Nishant Mohan et al. [23] blended aluminium nanoparticles into a mixture of diesel and biodiesel to investigate the emission and performance parameters of a CI engine. It was found that, at high loads, the performance showed a drop in maximum cylinder pressure and a 7% decrease in SFC in comparison with diesel. The addition of nanoparticles increased the exhaust gas temperature by 8% by increasing the BTE by about 9%, in contrast to diesel at maximum load conditions. The addition of nanoparticles reduced the emissions of CO by 25 to 40% and unburnt hydrocarbon by 8%, resulting in increased NO_x emission at high temperatures. Madhan Raj et al. [24] predicted the effects of aluminium oxide nanoparticle blends on the performance and emission characteristics of a CI engine. They blended fuel into different mass fractions, such as DF + Al₂O₃ 25 ppm and DF + Al₂O₃50 ppm, via a sonicator and used these to fuel the engine. They found that the addition of Al₂O₃ increases BTE with a decline in NO_x CO and HC emissions with different dosage levels of nanoparticles. The optimised fuel blend was found to be at a dose level of 50 ppm Al₂O₃. Prabhu L. et al. [25] analysed the emission and performance of CI engines fuelled with a mixture of titanium oxide (TiO₂) nanoparticles blended with a 20% biodiesel–diesel (B20) blend. The biodiesel blends contained 250 ppm and 500 ppm of titanium oxide nanoparticles. The results showed an increase in the BTE with reductions in emissions of hydrocarbons, carbon monoxide, and smoke opacity, while NO_x emissions were slightly increased for the B20TiO₂250 ppm blend when compared with pure B20 and the B20 TiO₂500 ppm blend at all load conditions. Pallavi Gogare et al. [26] examined the influence of the addition of aluminium nanoparticles on the emissions, combustion, and performance characteristics of a diesel engine running on diesel and biodiesel blends. From the results, it was observed that the BTE increases with the addition of Al₂O₃ nano-additives. The fuel blend B20 yielded a superior BTE, which was around 20.4%. Prabu Arockiasamy et.al. [27] used jatropha biodiesel and alumina nanoparticles in the base diesel fuel to investigate the performance, combustion, and emission characteristics of a diesel engine. The results of the experiments showed that, compared to pure biodiesel, the

JBD30A test fuel achieved a 9% reduced NO_x level, a 33% reduced unburned HC level, a 20% reduced CO level, and 17% reduced smoke opacity. Regarding the JBD30C test fuel, compared to neat biodiesel, there was a 7% reduction in NO_x, 28% reduction in unburned HC, 20% reduction in CO, and 20% reduction in smoke opacity. A 3.5% increase in BTE was observed for the JBD30A and JBD30C test fuels compared to neat biodiesel. Raja et al. [28] analysed the effects of an Al₂O₃–water nano-fuel used as a coolant on the heat transfer enhancement and NO_x emission in a CI engine. The investigation concluded that the use of nano-fluids resulted in a 12.5% decrease in NO_x emissions at full load and 3–5% at no load and partial load states. Ramarao et al. [29] examined the emissions and performance characteristics of CI engines fuelled with a mixture of CeO₂ nanoparticles, diesel, and biodiesel. The test fuels used in the study, and in different proportions, were B20, B20 + 0.04 gm CeO₂, B20 + 0.08 gm CeO₂, B50, B50 + 0.04 gm CeO₂, and B50 + 0.08 gm CeO₂. The results indicated that the added proportions of nanoparticles that enhanced the brakes' thermal efficiency and reduced harmful emissions of the optimised fuel to the greatest extent in terms of emissions and performance were found to be B20 + 0.08 gm CeO₂ and B20 + 0.04 gm CeO₂.

From the various studies in the literature, it may be noted that the addition of nanoparticles in diesel–biodiesel blends has a considerable impact on improving combustion and performance characteristics and reducing the emissions of CI engines. The addition of nanoparticles to biodiesel blends improves the performance and reduces the emissions of the dual-fuel engine, thereby providing a promising fuel source for diesel engines. Currently, the concern is not only energy but efficient conversion with global emissions reduction, which is of prime importance. As per the said Sustainable Development Goals (SDGs) 7 and 13, Fish Oil Methyl Ester (FOME), as a renewable resource, can effectively address the negative effects of fossil diesel fuel, such as its high import cost and subsequent foreign exchange burden, and the higher emissions of smoke, NO_x, and particulate matter arising from its use in engines. FOME can provide affordable, reliable, sustainable, and modern energy and address climate change and its impacts adequately. In the current study, the studied engine's fuel injector holes vary from three to four holes to enhance the rate of fuel mixing with air and reduce soot emissions; aluminium oxide nanoparticles are added to fish oil biodiesel, which is extracted from non-edible fish waste, thereby enhancing the physiochemical properties of the fish oil biodiesel; and the micro-explosion phenomenon and donation of extra oxygen atoms to the fish oil biodiesel results in complete fuel combustion and the enhancement of the engine's combustion characteristics.

2. Methods and Materials

2.1. Preparation of Fish Oil Methyl Ester

The fish oil methyl ester was prepared by preheating the waste fish oil and then via transesterification process, as described in Figure 1.

Initially, in the pre-treatment process, the solid impurities and a portion of water present in the waste fish oil were separated by a filter under a vacuum. The polar components such as lecithin, phospholipids, heavy metals, and pigments in the waste fish oil were removed by degumming them through phosphoric acid and water. Then, potassium hydroxide was added to remove free fatty acids such as soap in the oil in order to neutralise it. Finally, any other impurities and dyes were removed by the silica gel column chromatography technique. The sample was dried by heating it at 105 °C for 15 min.

The transesterification process takes place in two stages. Fish oil has a high level of free fatty acids above 15, so the transesterification process of residual fish oil is carried out in two steps. Figure 2 illustrates the stepwise preparation of fish oil biodiesel [30]. Due to its low cost, methanol is used as the alcohol for the transesterification process. In the first step, sulfuric acid (H₂SO₄) is used as the acid catalyst because it is more efficient at converting high free fatty acids (FFAs) to esters. The next step is the use of sodium hydroxide (NaOH) as an alkaline catalyst since it reacts faster and is more economical than an acid catalyst. Therefore, an acidic pre-treatment step including an alkaline catalysis

stage is applied to transform the residual fish oil samples into esters. Residual fish oil is converted to 12 methyl esters by an acid transesterification process with sulphuric acid (H_2SO_4) in the presence of methanol and a catalyst. For 1 L of the used fish oil, 300 mL of methanol and 15 mL of rigorous sulphuric acid (H_2SO_4) are used. This mixture is heated in a flask with constant stirring at 60 °C for 35 min; then, it is extracted and allowed to stand for 6–8 h in a decanter. Here, the acid esterification layer separates and must be removed from the oil. If the FFAs are removed, then the second step is completed. If the FFA concentration exceeds 4%, the same procedure as above is performed. For this reaction, the upper layer of the previous process, which is low in FFA, is used. The product obtained in the previous step, for example, the triglyceride, is reacted with methanol (200 mL) and NaOH (4 g) catalyst for 1 L of plum oil and heated at 60 °C with constant heating and stirring for 1 h. The reacted products of this phase will settle to the bottom of the gravel container. The lower layer contains glycerin and other impurities, which must be separated from the methyl ester.

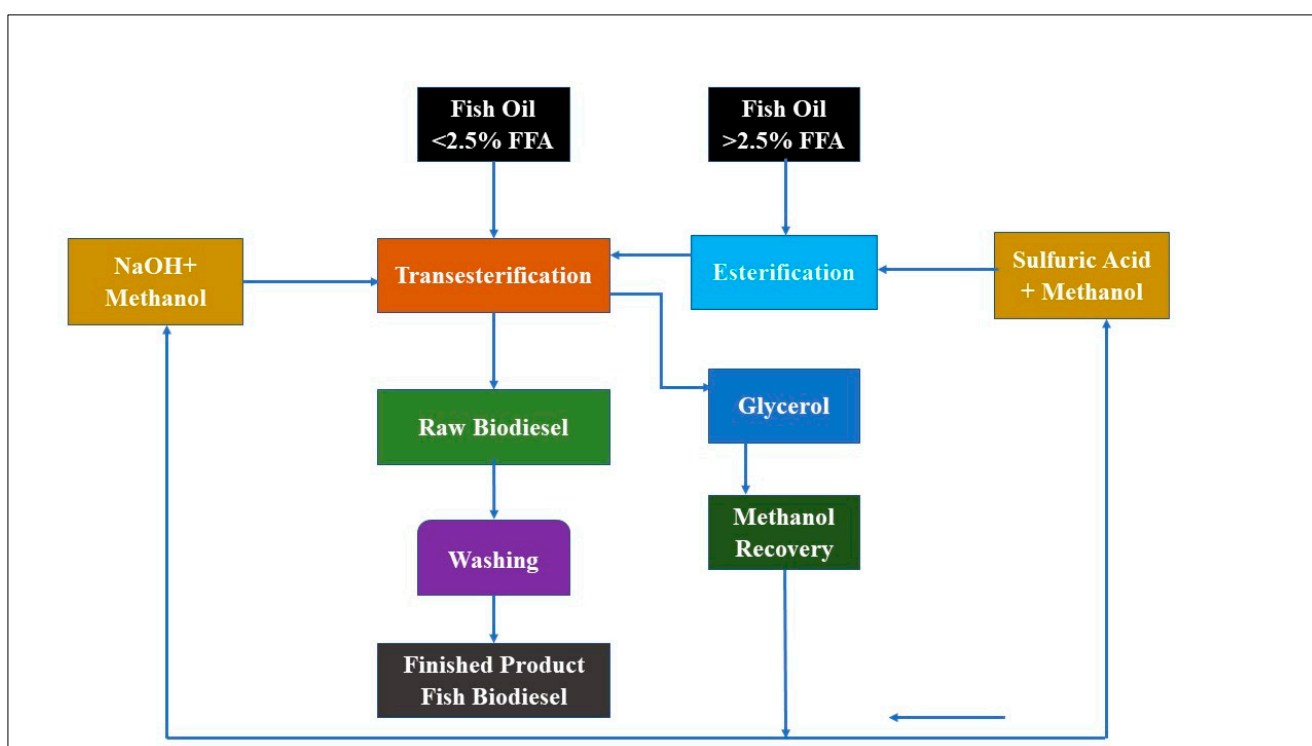


Figure 1. Transesterification reaction of Fish oil.

2.2. Alumina (Al_2O_3) Nanopowder

Aluminium oxide is commonly called alumina, and it is composed of two atoms of aluminium and three atoms of oxygen bonded together in a closed-loop hexagonal crystal structure (HCS) form. Table 1 illustrates the aluminium oxide nanoparticle specifications. Due to its availability in large quantities and abrasiveness, it is heavily used in various industries. Numerous techniques, such as the sol–gel process, pyrolysis, laser ablation and sputtering, are used to obtain alumina. These are generally observed in two forms: sphere-shaped single particles or tilting fibres. Alumina is obtained from two sources: bauxite ore and recycled alumina. The bauxite ore is the main source of alumina and is formed by mixing aluminium oxides such as magnetite (Fe_3O_4), quartz (SiO_2), hematite (Fe_2O_3), different non-metals, and metals. Aluminium oxide nanoparticles were procured from Sigma Aldrich Ltd. (St. Louis, MI, USA). Figure 3a illustrates Alumina (Al_2O_3) structure and Figure 3b shows the Micro-explosion phenomenon of nano-additives. Table 2 illustrates the test fuel properties.

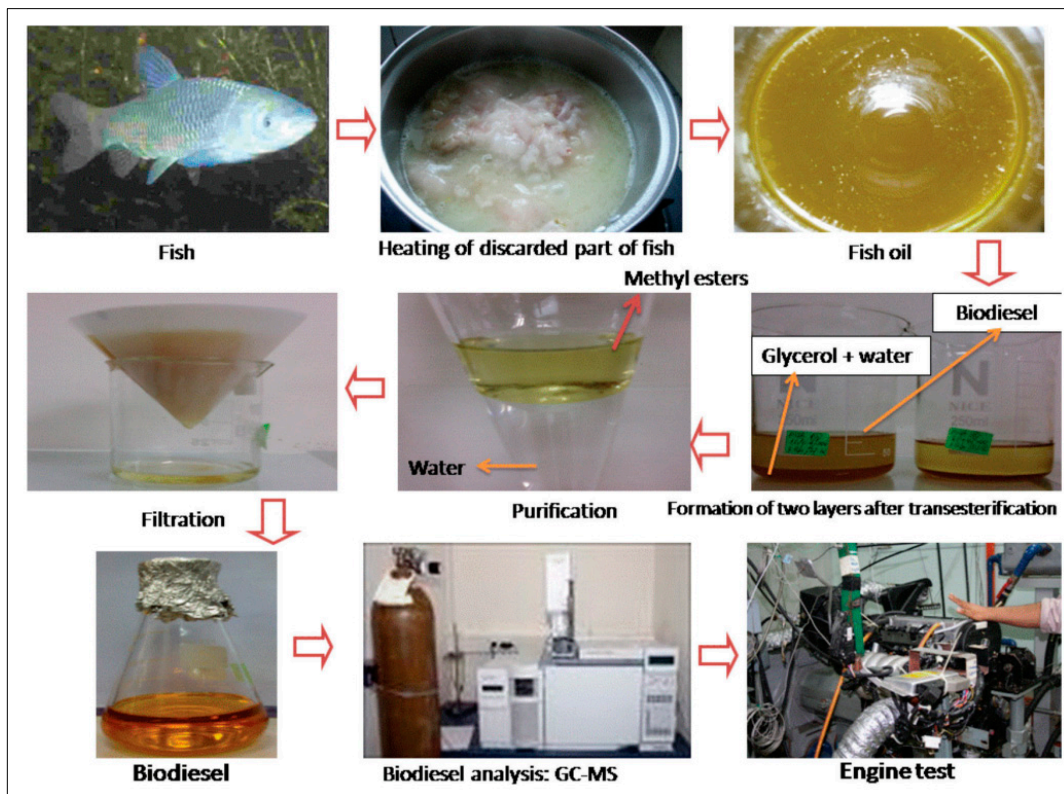


Figure 2. Step-wise preparation of fish oil biodiesel [30].

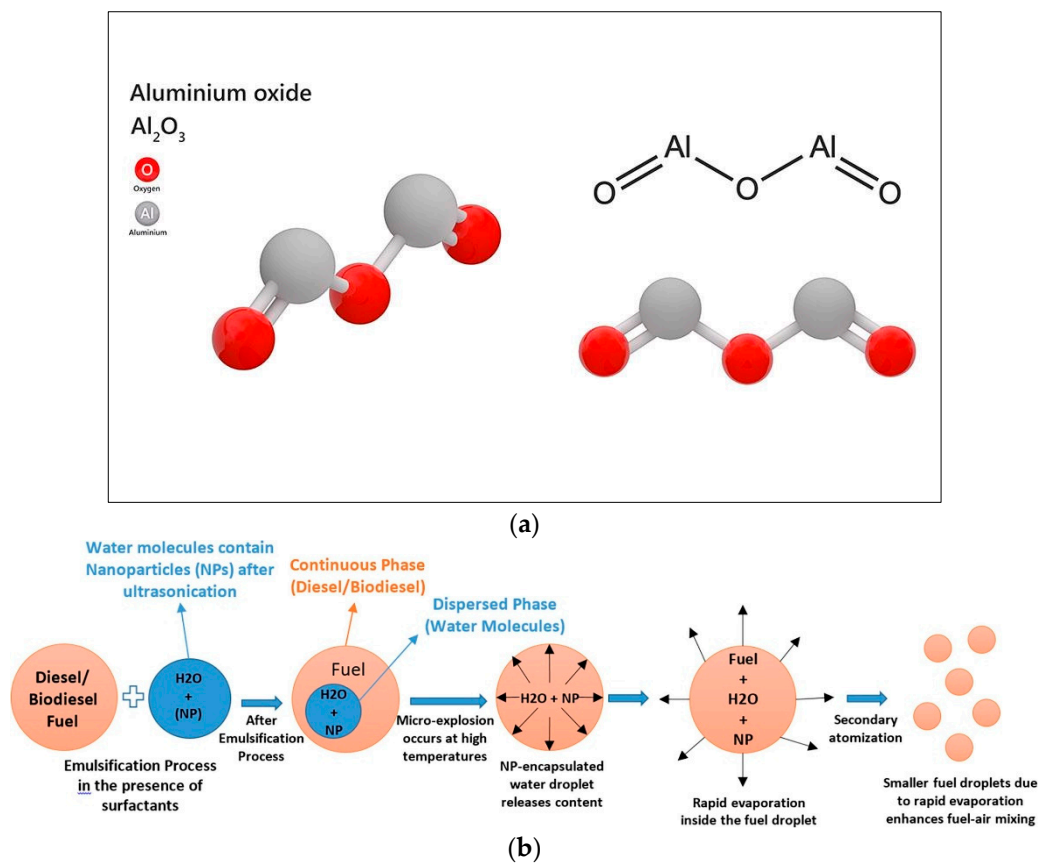


Figure 3. (a) Alumina (Al_2O_3) structure [31] and (b) Micro-explosion phenomenon of nano-additives [32,33].

Table 1. Aluminium oxide nanoparticle specifications.

S.No	Parameters	Specifications	ASTM
01	Composition	Oxide of Gamma aluminium (Al ₂ O ₃) in the gamma stage (99.9%)	ASTM E3001-20
02	Particle Size	20 to 50 nm	
03	Colour	White	
04	Melting point	2045 °C	
05	Density	3.9 g/cm ³	
06	Boiling point	2980 °C	
07	Surface Area	155 m ² /g	

Table 2. Test fuel properties.

ASTM Standard	Property	Diesel	Fish Oil	Fish Oil Biodiesel
D445	Kinematic viscosity at 40 °C	3.08	24.32	3.78
D4052	Density, kg/m ³	828	898	878
D93	Flashpoint, °C	60	194	160
D93	Fire point, °C	65	198	165
D613	Cetane number	40	48	80
D5865	Calorific Value, MJ/kg	46	3608	38

3. Experimental Setup

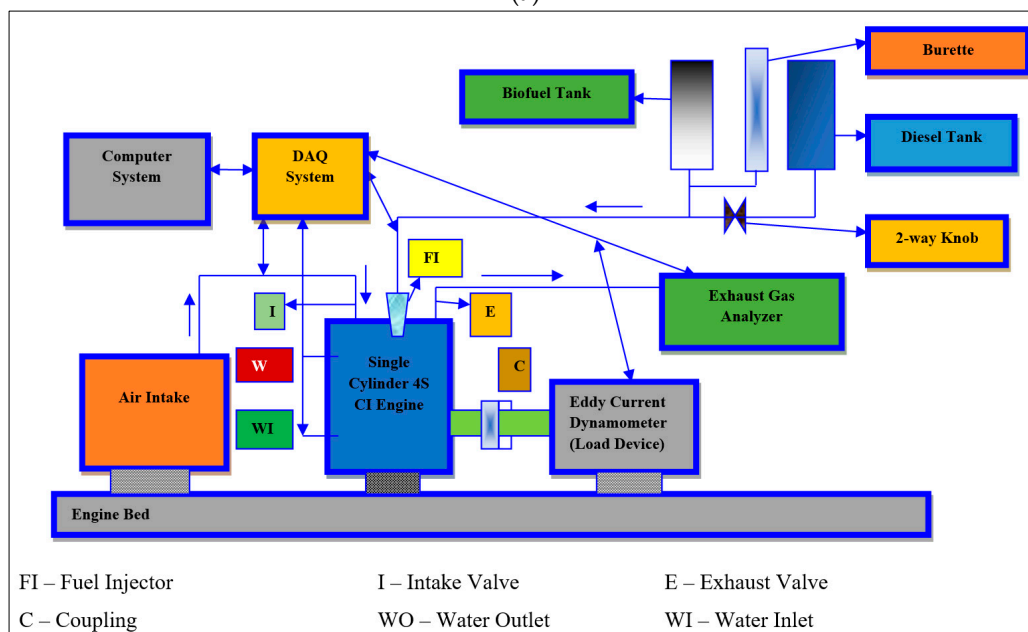
In this experiment, the Kirloskar TV1-type single-cylinder diesel engine was fuelled by FOME biodiesel, and a pure diesel mixture with the addition of aluminium oxide nanoparticles (Al₂O₃) was used to analyse the effects of the injection pressure and aluminium oxide nano-additives on the emissions and BTE of the compression ignition engine. The experimental arrangement used is depicted in Figure 4a, while a schematic presentation is shown in Figure 4b, which was derived from Ahmed SA and Soudagar et al. [34], and its specifications are given in Table 3.

Table 3. Test engine's specifications [35].

TV1 Kirloskar Engine	Specifications
No. of cylinders	1
No. of strokes	4
Fuel type	Diesel
Speed	1500 rpm
Rated power	3.5 kW
Bore	80 mm
Diameter of injector orifice	0.20 mm, 0.25 mm
Length of Stroke	110 mm
Connecting rod length	234 mm
Type of Cooling	Water-cooled
Compression ratio	17.5:1
Arm length of the Dynamometer	185 mm
Type of loading	Mechanical



(a)



(b)

Figure 4. Experimental setup: (a) pictorial presentation; (b) schematic presentation [34].

3.1. Fuel Injector

The fuel injectors used in this study are shown in Figure 5 and the specifications are given in Table 4. Diesel is injected at 205 bar, which is lower than that used for biodiesel. This is due to its lower viscosity compared to the latter. Biodiesel has comparatively higher viscosity; hence, it needs to be injected at higher injection pressure of 240 bar. Both the pressures adopted for diesel and biodiesel are optimised values in terms of maximised engine performance coupled with lower emissions. The injection pressure is varied by adjusting the spring stiffness of the injector nozzle and the prerequisite pressure to be set is measured by using a nozzle tester as shown in Figure 5.

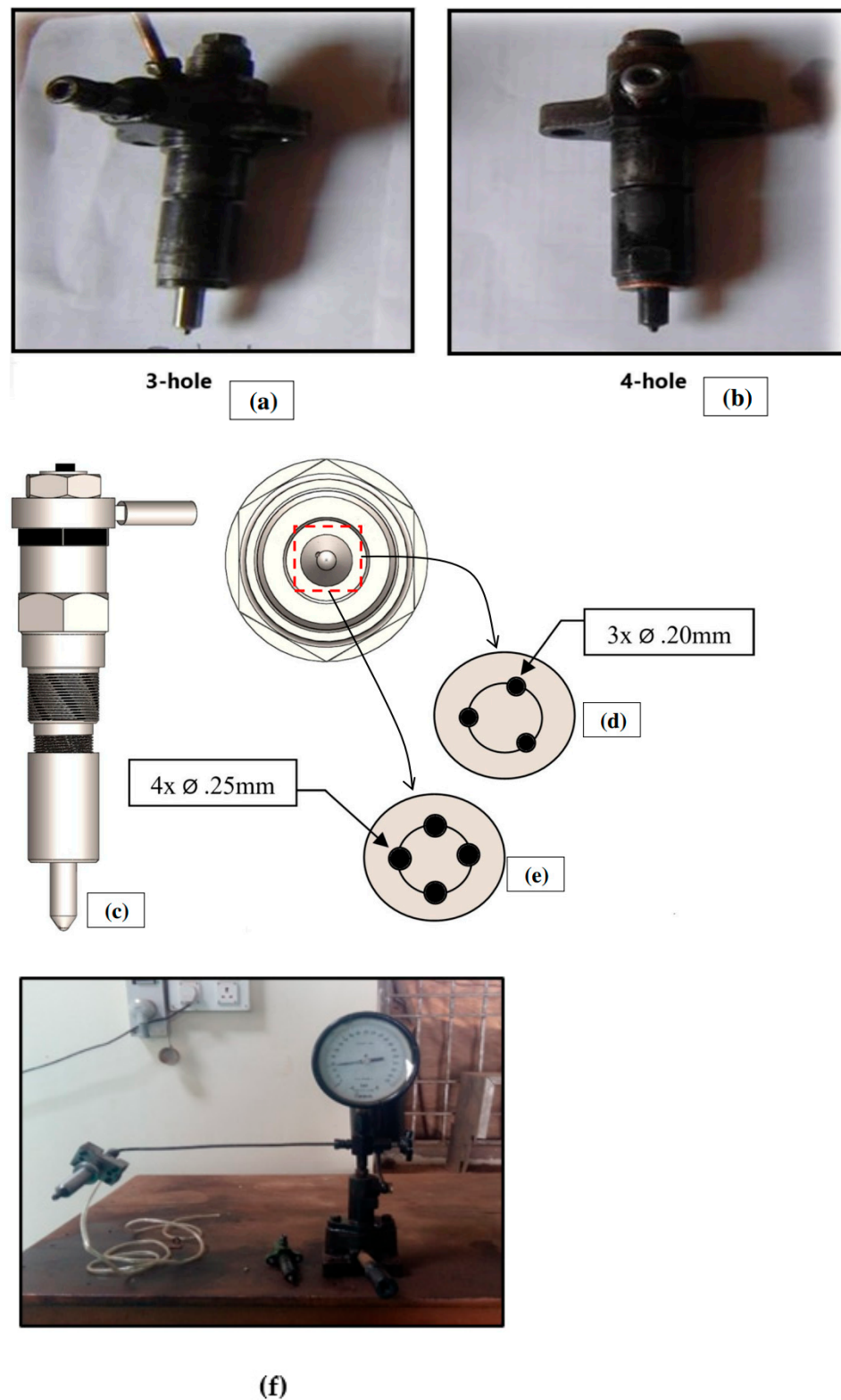


Figure 5. (a–e) The 3- and 4-nozzle hole fuel injectors [36]; (f) injector pressure tester.

Table 4. Specifications of fuel injectors used.

S.No.	Number of Holes	diameter of Hole in mm
1	3 holes	0.20 mm
2	4 holes	0.25 mm

3.2. Test Fuel Blends and Nano-Biodiesel Blend Preparation

The nano-diesel preparation steps are followed to obtain a stable blend. Accordingly, the weights of the nanoparticles and liquid fuels are measured using precision scales. Then, the nanoparticles are dispersed into the diesel–biodiesel blends. In this step, a mechanical stirrer was used at 500 rpm for 30 min. Then, the nanoparticle-added diesel–biodiesel blends were exposed to ultrasonication waves at 40 kHz for 120 min. The temperature of the ultrasonic bathwater was kept at 25 °C during all ultrasonication processes. Consequently, stable nano-diesel fuels were obtained and then poured into the fuel tank to stop the nanoparticles in the liquid fuels from settling [36]. Figure 6a illustrates the comprehensive steps involved in the preparation of nano-fuel blends.

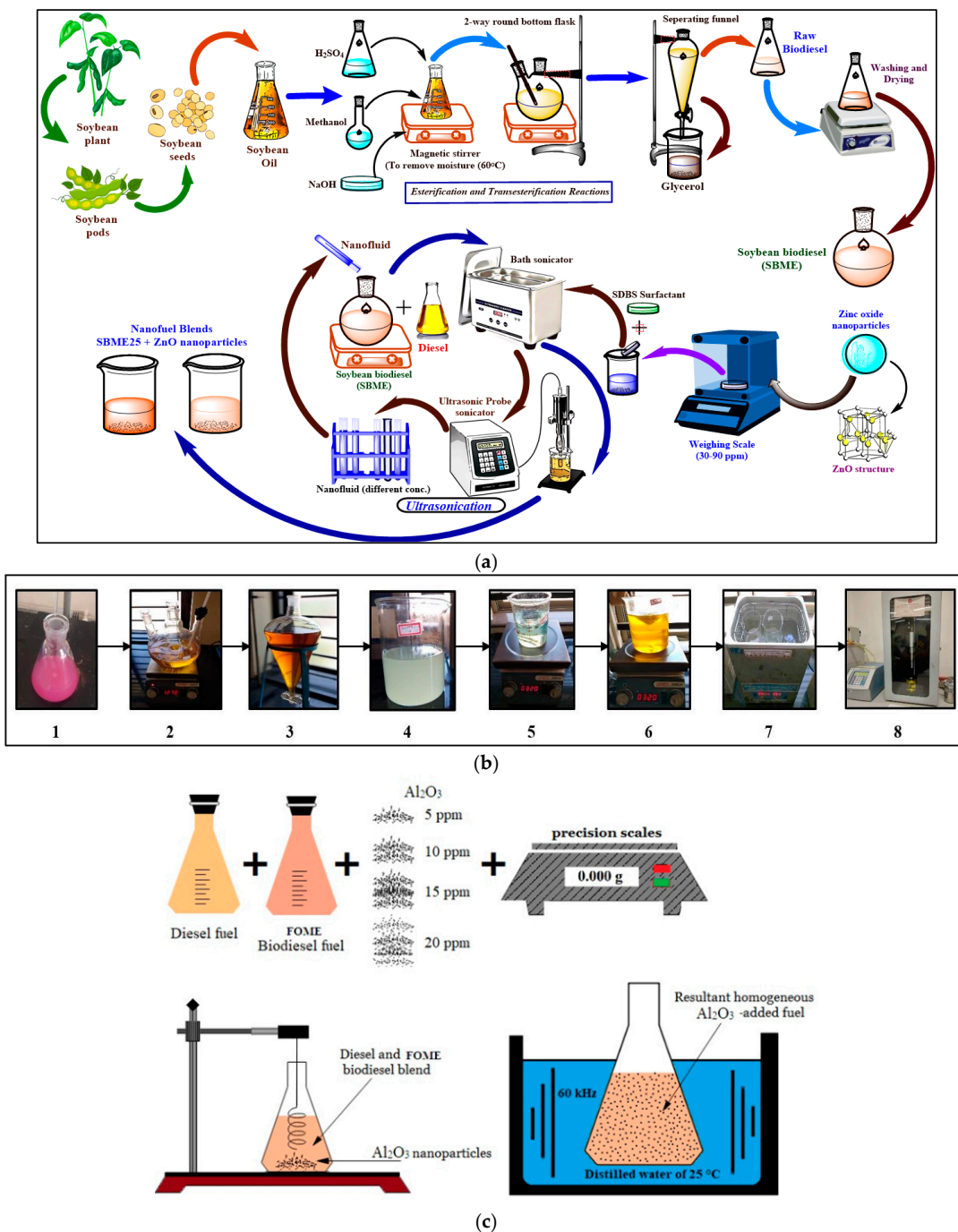


Figure 6. (a) Preparation of nano-fuel blends [37], (b) stepwise preparation of nano-fuel blends [38], and (c) FOME–Aluminum oxide nano-fuel preparation steps [36].

3.3. Experimental Procedure

Firstly, the properties of fuel such as viscosity, the fire point, density, and the flash point were determined through various apparatuses. As described in Table 5, the nano-diesel blends were prepared in different proportions. The engine was started by cranking, and, after 3 to 4 min, the load was applied. The experiment was repeated under different loads and different test fuel blends. For all the tabulated readings, calculations were performed to plot the performance and emission graphs. Lastly, the conclusion was made by analysing graphs and the optimised fuel blend was suggested with respect to providing a superior BTE and reducing exhaust emissions.

Table 5. Specifications of exhaust gas analyser.

Type	DELTA 1600S
Object of Measurement	Carbon monoxide (CO), Carbon Dioxide (CO ₂) and Hydrocarbons (HC)
Range of Measurement	HC = 0 to 20,000 ppm as C ₃ H ₈ (Propane) CO = 0 to 10%, CO ₂ = 0 to 16%, O ₂ = 0 to 21% NO _x = 0 to 5000 ppm (as Nitric Oxide)
Accuracy	HC = +/- 30 ppm HC CO = +/- 0.2% CO, CO ₂ = +/- 1% CO ₂ O ₂ = +/- 0.2% O ₂ NO _x = +/- 10 ppm NO
Resolution	HC = 1 ppm, CO = 0.01% Vol. CO ₂ = 0.1% Vol., O ₂ = 0.01% Vol. NO _x = 1 ppm
Warm-up time	10 min. (self-controlled) at 20 °C
Speed of Response Time	Within 15 sec. for 90% response
Sampling	Directly sampled from tail pipe
Power Source	100 to 240 V AC/50 Hz
Weight	800 g
Size	100 mm × 210 mm × 50 mm

3.4. Analysis of Uncertainty

Systematic equations are used to analyse the error estimations of the investigative data. The average of the measured factors is used in the uncertainty analysis to determine the real value. Table 6 illustrates the accuracy levels of the engine parameters. Equation (1) is used to compute the total uncertainty

$$\frac{U_y}{y} = \sqrt{\sum_{i=1}^n \left(\frac{1}{y} \frac{\partial y}{\partial x_i} \right)^2} \quad (1)$$

where 'y' is a specific factor that relies on the parameter 'xi' and U_y indicates the level of uncertainties or variation in 'y'.

The uncertainty propagation for two or more independent parameters specified by the factors is applied as follows in Equation (2):

$$\frac{U_y}{y} = \sqrt{\left(\frac{u_{x_1}}{x_1} \right)^2 + \left(\frac{u_{x_2}}{x_2} \right)^2 + \dots + \left(\frac{u_{x_n}}{x_n} \right)^2} \quad (2)$$

where U_y—uncertainty; y—test value; x₁, x₂, ..., x_n—assessed parameter(s); and uncertainty of emissions is $U_y = \frac{\text{Resolution}}{\text{Range}}$.

Table 6. Accuracy levels of engine parameters.

Parameters	Accuracy (\pm)
CO emission (%)	$\pm 0.01\%$
NOx emission (ppm)	± 10 ppm
UBHC emission (ppm)	± 10 ppm
Exhaust gas temperature ($^{\circ}\text{C}$)	± 1 $^{\circ}\text{C}$
Smoke meter (HSU)	$\pm 0.1\%$
Pressure Transducer (bar)	± 0.1 bar
Dynamometer load cell (g)	± 50 g
Engine speed (rpm)	± 10 rpm
Measuring Burette (cc)	± 0.25
Crank angle encoder ($^{\circ}\text{CA}$)	$\pm 1^{\circ}$

The overall uncertainty is defined as follows:

$$\begin{aligned}
 &= \sqrt{\text{Uncertainty (\%)} \text{ of } (\text{Engine speed}^2 + \text{CO emission}^2 + \text{NOx emission}^2 + \\
 &\quad \text{HC emission}^2 + \text{Brake thermal efficiency (BTE)}^2 + \\
 &\quad \quad \quad \text{+Smoke}^2)} \\
 &= \sqrt{\text{Uncertainty (\%)} \text{ of } (0.6^2 + 0.6^2 + 0.7^2 + \\
 &\quad \quad \quad 0.5^2 + 0.7^2 + \\
 &\quad \quad \quad 0.5^2)} \\
 &= \pm 1.45
 \end{aligned}$$

4. Results and Discussion

The obtained experimental data are used for the analysis of the BTE; emissions such as CO, NO_x, and HC; and the smoke density of the test fuels.

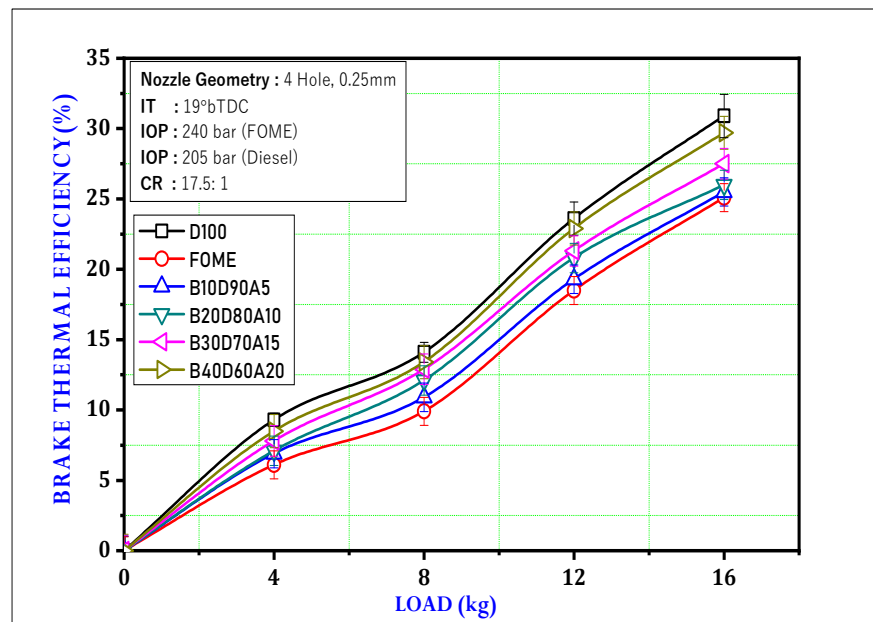
4.1. Performance Analysis—Brake Thermal Efficiency Variation with Load

Figure 7a,b illustrate the variation in the BTE with load for three holes at 240 and 260 Bar, respectively, for the blends of diesel, FOME, and Al₂O₃ nanoparticles.

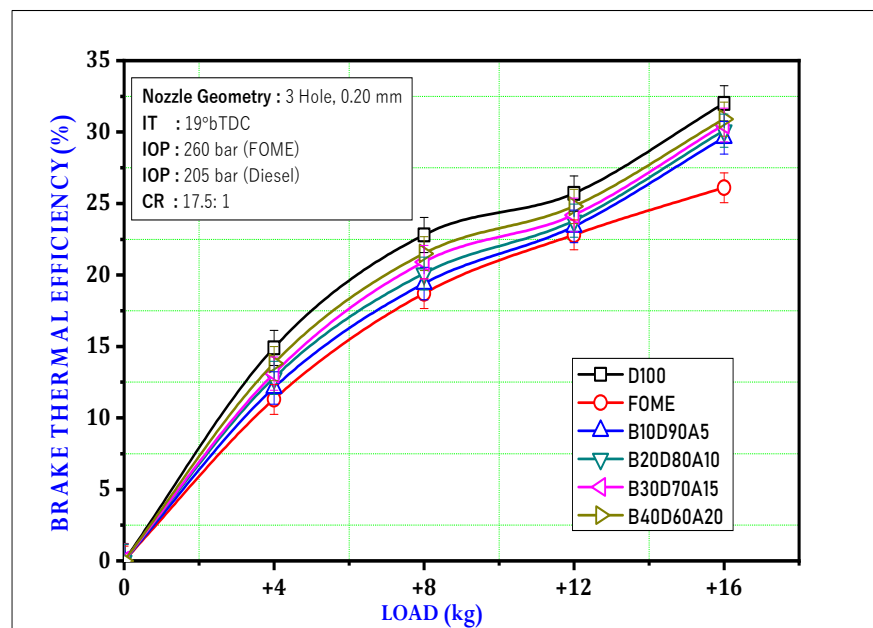
From the two graphs, it can be inferred that as the engine load increases, the value of the BTE for all test fuel combinations increases. This trend is attributed to the frictional force, which remains constant at minimum and maximum loads but is negligible with increasing power at maximum loads. Therefore, the loss of frictional forces is lower during piston movement at high loads on the engine, which improves the performance of the engine at high loads. One more significant reason for the enhanced BTE might be related to the increase in cylinder temperature at peak loads. Comparing this with a lower engine load, more fuel is required to attain high engine loads. Considering all the experimental mixtures collectively, it can be seen in both figures that a high brake thermal efficiency is consistently obtained for diesel fuel.

In both figures, it can be seen that the BTE decreases sharply as the engine is run on FOME fuel. The main reason behind the variation is possibly due to the CV of the test fuels, as shown in Table 4. From the table, we can observe that diesel has a higher CV than FOME, resulting in a notable decrease in BTE when the FOME fuel is used. One more reason why the BTE drops with FOME can be attributed to the viscosity of the fuel (Table 4) [6,20]. The viscosity of FOME is higher than that of diesel fuel, resulting in poor injection characteristics for FOME. This is due to the diameter of the fuel droplets of high-viscosity fuels being larger and, therefore, possessing poor atomization. Thus, the delay period becomes longer

and the other parameters of combustion worsen. All of these possibilities can reflect a reduction in the BTE for FOME fuel.



(a)



(b)

Figure 7. (a) BTE Variation with load for 3 holes at 240 Bar. (b) BTE Variation with load for 3 holes at 260 Bar.

When Al_2O_3 is added to the test fuel, it has been observed that the performance enhances with the increasing mass fraction of Al_2O_3 in the test fuel. As a result, the better BTE progress was at a set load when the engine was fuelled by the B40D60A20 test fuel in both cases. The cause for the BTE progress via the addition of Al_2O_3 nanoparticles is the higher surface-to-volume ratio of the nanoparticles, which leads to an increase in the catalytic role [6,20]. In this way, the chemical reactions throughout ignition are accelerated

and ensure an additional duration of combustion of the unburned fuels [39]. Overall, thermal efficiency is improved. Another reason for the increased energy presence in the test fuels is the addition of Al_2O_3 nanoparticles in the fuels. Therefore, according to Figure 7a, it was found that the B40D60A20 test fuel indicated superior brake thermal efficiency of 29.3%, which was 16.38% superior to the FOME and 3.75% lower than diesel at maximum load for a 240 bar injection pressure. When the pressure of injection is increased to 260 bar, an increased BTE was observed compared to the injection pressure at 240 bar. The proper atomization, correct air–fuel mixture, and augmented evaporation rate properties made diesel fuel exhibit a superior BTE compared to all the other test blends [40]. Accordingly, from Figure 7b, it was found that, out of all the test blends, the B40D60A20 test fuel indicated the highest brake thermal efficiency of 30.7%, which is 15.63% superior to the FOME fuel and 3.90% less than diesel at maximum load [41]. These findings matched those previously obtained in the literature [39,42–44]

4.2. Performance Analysis—Brake Thermal Efficiency Variation with Load

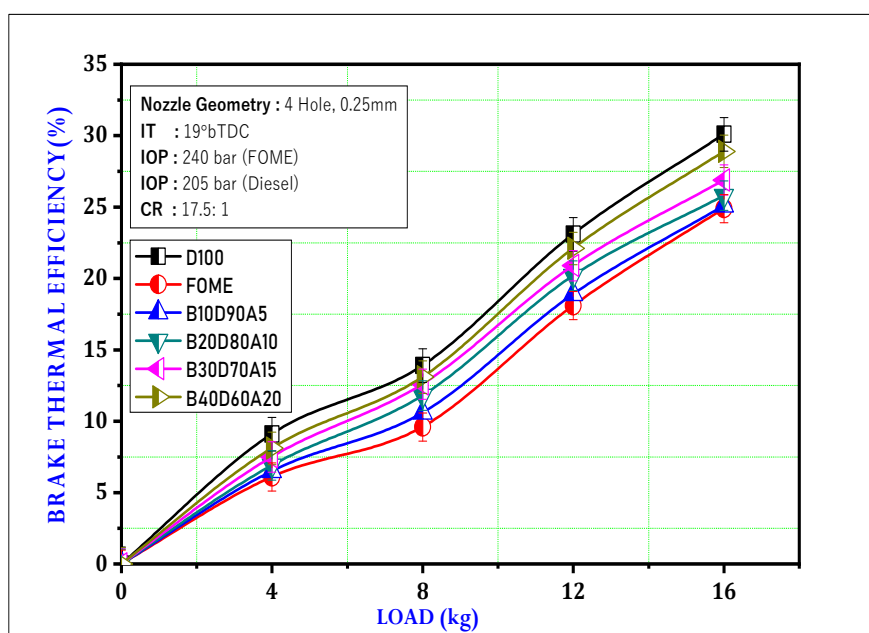
Figure 7a,b illustrate the deviation of the BTE with load for four holes at 240 and 260 bar, respectively, for the blends of diesel, FOME, and Al_2O_3 nanoparticles. From both graphs, it can be seen that the BTE for a four-hole fuel injector decreases in comparison with a three-hole fuel injector. The cause for the enhancement in the BTE might be attributed to the injection parameters with a three-hole injector of diameter 0.20 mm. The hole numbers and the diameter of the injector nozzle are valuable factors which sturdily influence the injection parameters of the test fuels. The smallest nozzle diameter used has small-diameter fuel droplets, as presented in Figure 8. Correspondingly, as the injector nozzle's diameter increases, the diameter of the fuel droplets also increases. Accordingly, the atomised fuel takes a longer time to evaporate, resulting in a longer ignition delay. The burning time decreases as the ignition and dwell period becomes longer. As a result, the fuel does not have enough time to burn completely, which deteriorates the brakes' thermal efficiency [39]. This demonstrates how the BTE drops for the smaller diameter of the injector nozzle. To have a clear picture in mind, the following scheme is presented in the study. When the BTE is compared at 240 bar and 260 bar, the BTE at 260 bar increases as compared to the BTE at 240 bar because of increased pressure. From both graphs, the maximum BTE is observed for the B40D60A20 blend, which is 29.9%, and it is 14.38% superior to FOME and 4.34% inferior to diesel at an average load. The reason for the increase in the BTE is the Al_2O_3 nanoparticles' properties such as better atomization, an increased rate of evaporation, and a high surface area to volume ratio, which enables the total combustion of fuel. Figure 8c illustrates the fuel droplet diameter and atomization as per the nozzle diameter. These findings matched those in the literature [45,46].

4.3. Emission Comparison—Carbon Monoxide Emission

Figure 9a,b illustrate the variation in CO emissions with load for the blends of diesel, FOME, and Al_2O_3 nanoparticles at three-hole and four-hole nozzle geometries, respectively. It is observed from both graphs that diesel fuel presented reduced CO emissions because of its larger calorific value, low viscosity, and high heat release rate. The FOME provided the utmost CO emissions as it has a high viscosity, better density, and rich air–fuel mixture [47,48]. The slower rates of oxidation and combustion, comprising the calorific value of fuel, are improved by the addition of aluminium oxide nanoparticles to FOME, which also lowers CO emissions.

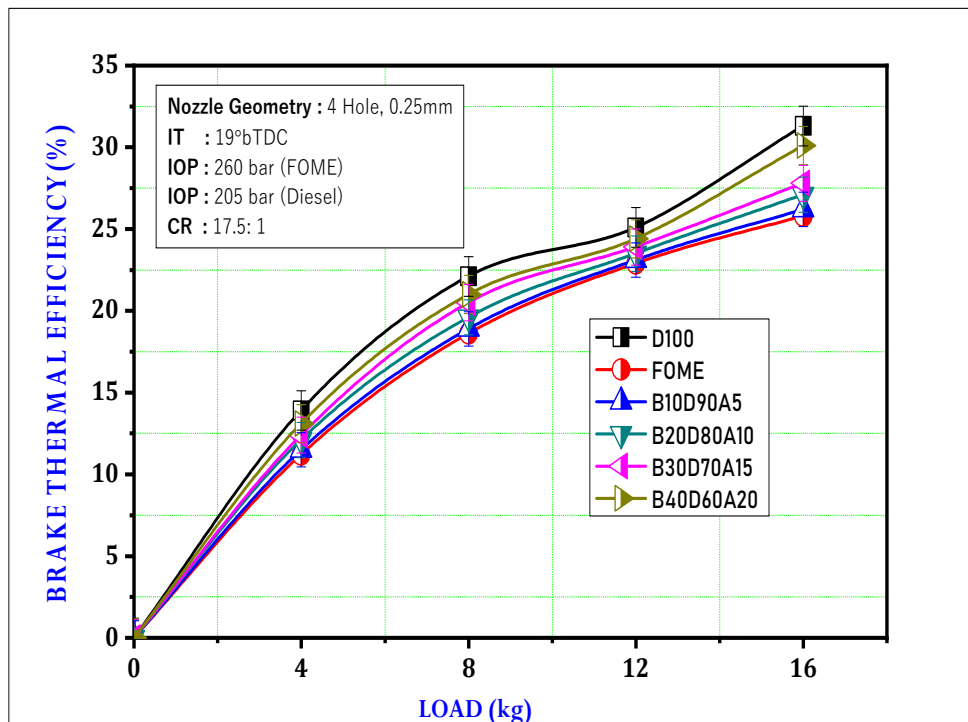
It can be seen from Figure 9b that there is a reduction in CO emissions for each B10D90A5 blend by 13.51%, for B20D80A10 by 16.21%, for B30D70A15 by 27.02%, and for B40D60A20 by 43.24% as compared to FOME. In addition, the CO emissions are comparable to diesel at all loads for the blend B40D60A20 [49]. From Figure 9a, it is evident that the blends B10D90A5, B20D80A10, B30D70A15, and B40D60A20 yielded reduced CO emissions by 9.67%, 12.90%, 25.80%, and 48.38% in comparison with FOME. In addition, the CO emissions of the blend B40D60A20 are comparable to diesel at the given load range.

The CO emissions drastically drop with the addition of Al_2O_3 nanoparticles due to the nanoparticles' substantial catalytic effect. Nanoparticles ensure a superior surface area–volume ratio and lower fuel consumption. Nanoparticles accelerate chemical reactions as they have a higher degree of catalytic action for the duration of the burning process and decrease the activation energy essential for the commencement of reactions. Hence, for the duration of the combustion process, chemical reactions occur at lower temperatures with the quickening of these reactions, and there is a possibility of the re-oxidation of unburned fuels during the combustion period. Due to this occurrence, unburned fuels are once again oxidised and the levels of products of inadequate combustion such as CO and H_2 are reduced through the addition of nanoparticles. Through the increase in the nanoparticle dosage, the reduction in CO emissions was also obvious. The cause for the increase in the dose of nanoparticles is an increase in the number of free-flow nanoparticles in the fuel and the resulting increased catalytic effect. Further, the lowest CO emission was noticed for the B40D60A20 fuel, which contained the maximum dosage of Al_2O_3 nanoparticles. Both graphs show that the CO emissions are high for four-hole injectors compared to the three-hole injectors due to their uneven geometry. The fundamental reason behind the reduction in CO emissions with the 0.20 mm diameter three-hole injector might be attributed to the improved injection parameters. When the nozzle diameter is smaller, smaller diameter droplets of fuel can be sprayed. For this case, the surface area to volume ratio of the fuel droplets increases, thereby enabling greater fuel oxidation. As a result, CO emissions were recorded when the engine is running with a 0.20 mm diameter three-hole nozzle. On the contrary, the larger the diameter of the fuel droplets, the better the ratio of the surface area to volume, which reduces fuel oxidation. Moreover, it was noticed that the CO emissions reached their maximum value with increasing loads for a specified test mixture because of the increase in fuel consumption at high engine loads. Engine speed and air intake were stable throughout the experiment. Therefore, as the load on the engine increases, the air–fuel ratio varies owing to the augmented consumption of fuel. Thus, the CO emissions increase sharply at high loads as they do not have enough time to oxidise completely. Regardless of the nozzle hole numbers and the diameter, CO emissions show comparable trends as a function of load variation. Related trends were observed in previous studies [49–51].

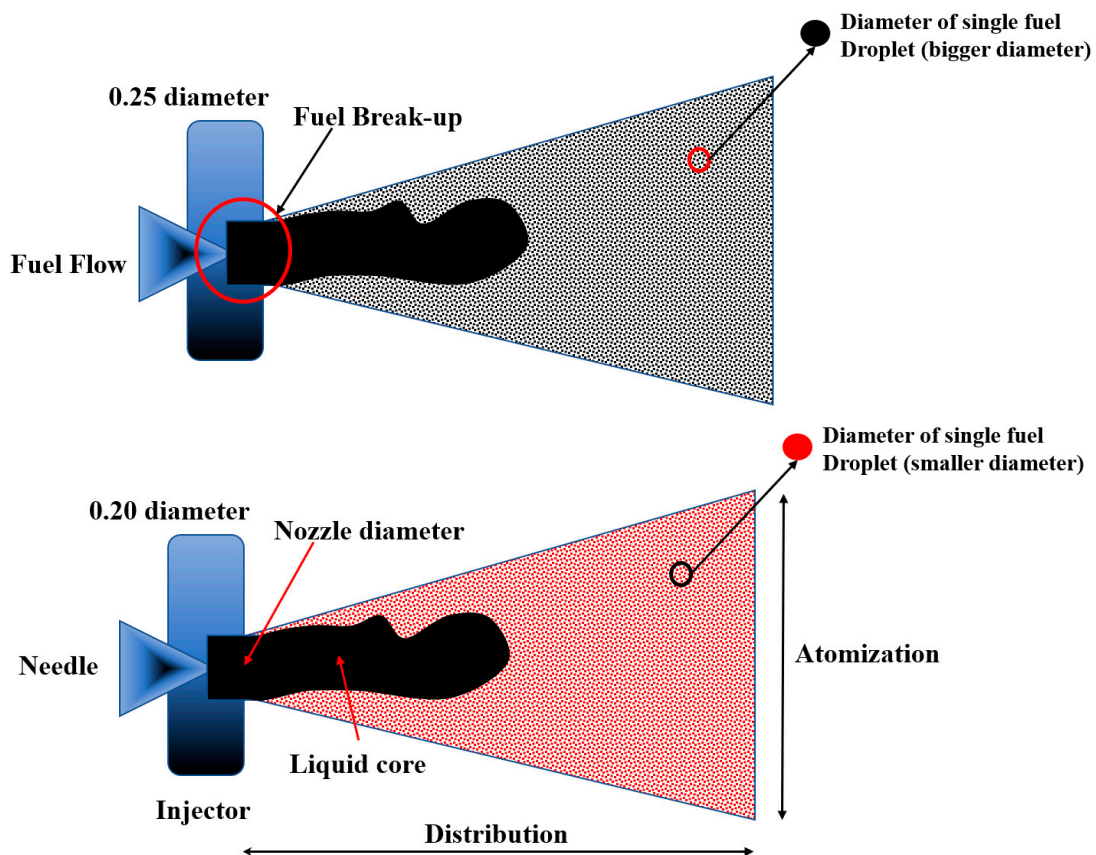


(a)

Figure 8. Cont.

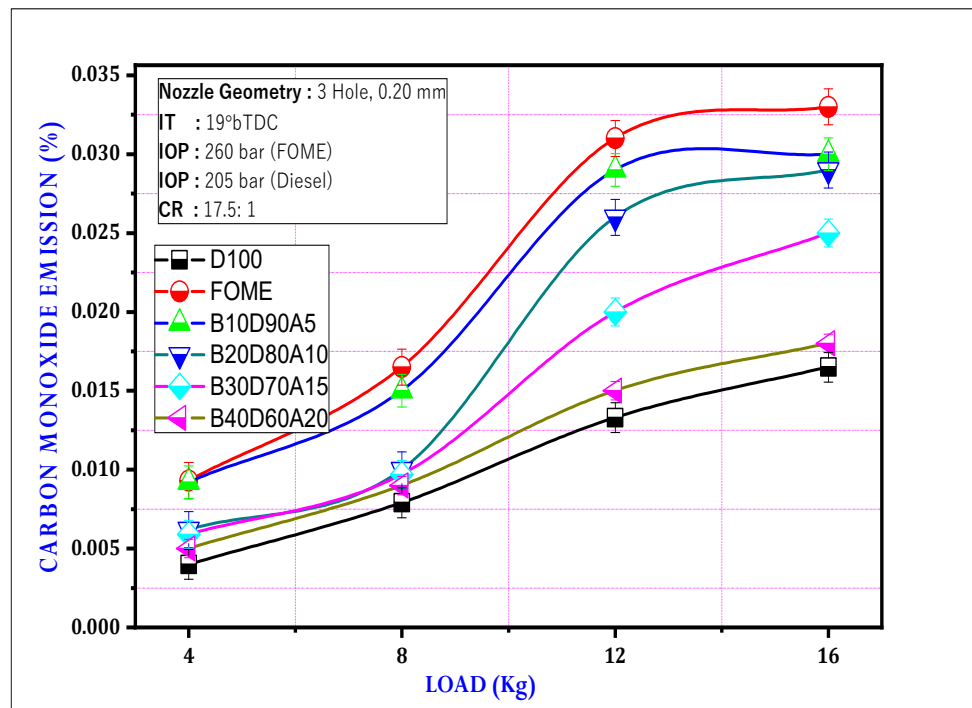


(b)

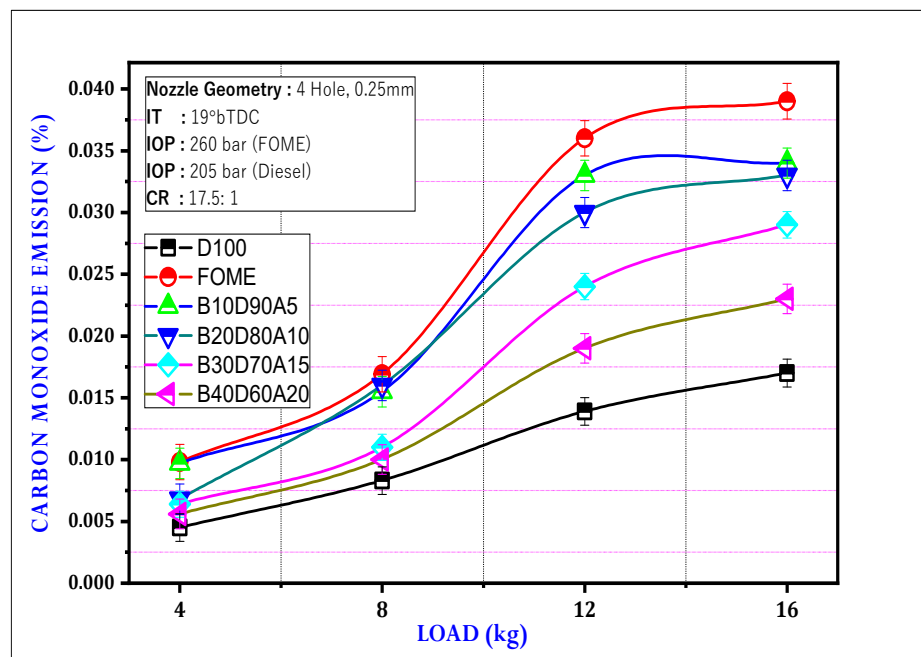


(c)

Figure 8. (a) BTE Variation with load for 4 holes at 240 bar. (b) BTE Variation with load for 4 holes at 260 bar. (c) Fuel droplet diameter and atomization as per the nozzle diameter [36].



(a)



(b)

Figure 9. (a) CO emission variation with load for 3-hole nozzle geometry. (b) CO emission variation with load for 4-hole nozzle geometry.

4.4. Emission Comparison—Hydrocarbon Emission

Figure 10a,b illustrate the variation in HC emissions with load for the diesel, FOME, and Al₂O₃ nanoparticle mixtures with three- and four-hole nozzles, respectively. Similar to CO emissions, HC emissions are also products of incomplete combustion and decrease as combustion progresses to completion. The important parameters concerning HC emissions

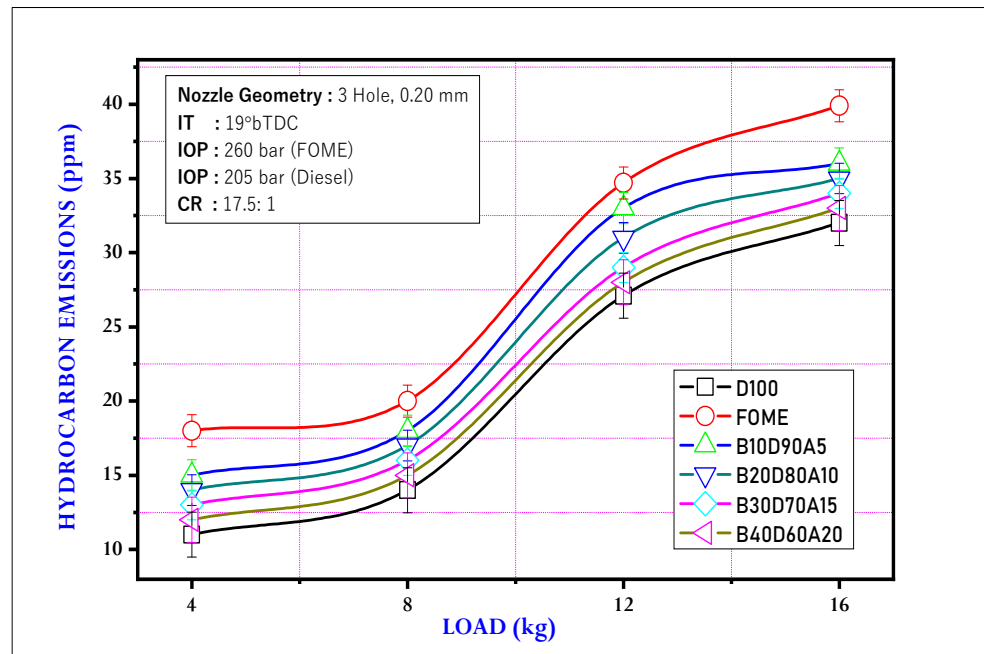
are the air/fuel ratio, the chemical composition (C, H, and O) of the fuel, the supply of adequate oxygen for the fuel's oxidization during combustion, and other thermo-physical properties of the fuels such as their calorific value, cetane number, viscosity, etc. These all are considered vital parameters responsible for the hydrocarbon emissions of internal combustion engines. With the variation in engine load, the HC emissions trend is similar to that of CO emissions. Thus, as the engine load increases, the degree of incomplete combustion increases, leading to increased CO and HC emissions. Hence, the highest HC emissions were detected at the point where the highest CO emissions were recorded. The cause for this is the lower heating value and higher viscosity of FOME, which results in the inferior combustion and increased fuel consumption for the test fuel. Subsequently, the HC emissions are reduced by the addition of the Al_2O_3 nanoparticles in the fuel. The key cause for this might be the catalytic effects of the nanoparticles. As a result, the nanoparticles promote the oxidation of the fuel being tested, leading to complete combustion and improved performance. The addition of Al_2O_3 nanoparticles to the fuel mixture burns carbon particles because of the large surface catalytic activity in the cylinder and reduces HC emissions [52,53]. From Figure 10a,b, it can be seen that the HC emissions are greater for the four-hole fuel injectors compared to the three-hole fuel injector. Regarding the four-hole fuel injector, out of all the blends, blend B40D60A20 presented a reduced HC emission that is 20.42% inferior to that of FOME and 2.98% inferior to that of diesel. Alternatively, for the three-hole fuel injector, out of all the blends, blend B40D60A20 indicated a reduced level of HC emissions that is 17.51% inferior to that of FOME and 3.07% inferior to that of diesel. Researchers from the literature have presented similar trends in HC emissions [10,53].

4.5. Emission Comparison—Nitrogen Oxide Emissions

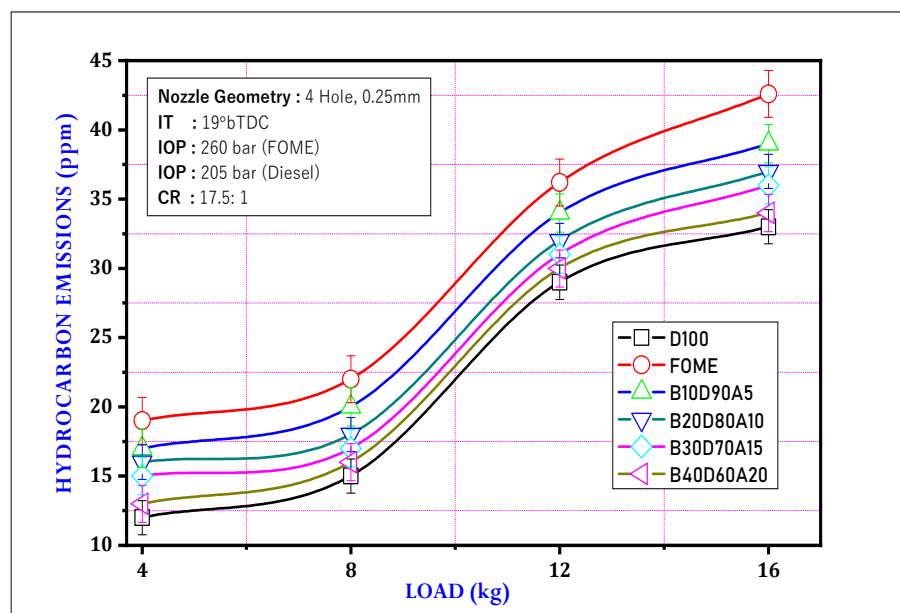
Figure 11a,b illustrate the variations in NO_x emissions with load for the blends of diesel, FOME, and Al_2O_3 nanoparticles at three-hole- and four-hole nozzle geometries, respectively.

The most critical parameter affecting NO_x emissions is the temperature during combustion. Generally, conventional fuels do not contain nitrogen and oxygen in their composition, but the air drawn to the cylinder to combust the fuel, which contains nitrogen and at higher temperatures, leads to NO_x formation. The level of NO_x formation increases since the reaction potential of nitrogen and oxygen atoms is higher at high temperatures [10,54]. Therefore, analyses in the literature use the exhaust temperature or the in-cylinder temperature, which reflects the former value, to explain the formation of NO_x . According to the analysis, the highest level of NO_x emission was measured for the FOME fuel. When the engine was solely fuelled by FOME, the fuel consumption was higher than the other fuels tested. The same trend was observed in the BTE study. While the engine must use more fuel to reach the same load, the temperature in the cylinder also rises when the engine runs on FOME fuel because of the surplus fuel being burned. Here, inside the combustion chamber, the oxygen and nitrogen particles take part in further reactions and the level of NO_x emission increases. Later, a considerable decrease in NO_x emissions was found via the addition of nanoparticles. The most important reason for this is the increase in fuel energy density, which causes a decrease in the consumption of fuel when nanoparticles are added to test fuels [39]. Moreover, the nanoparticles' higher thermal conductivity accelerates heat transfer and limits the formation of NO_x inside the combustion chamber. Thus, the greatest NO_x reduction is observed when the engine is fuelled by 20 ppm of Al_2O_3 nanoparticles. Among all mixtures for the nozzle with three holes and a 0.20 mm diameter, the mixture B40D60A20 showed NO_x emissions that were 22% lower than diesel and 16.52% lower than FOME biodiesel. Similarly, with respect to all mixtures for the nozzle of four holes and a 0.25 mm diameter, the mixture B40D60A20 indicated a NO_x emission level 3.11% lower than that of diesel and 25.10% lower than that of the FOME biodiesel. It has been observed that the engines fitted with a larger nozzle diameter produced lower NO_x emissions. The reason for this is that the larger-diameter fuel droplets at large nozzle diameters have better fuel atomization and shorter burn times due to a longer delay period. The larger-diameter

droplets of the atomised fuel interfered with the combustion course. In addition, as the fuel could not be completely burnt, it was discharged with exhaust without combustion, and the increase in temperature was relatively lower for this case. The lower temperature was also responsible for a drop in the degree of NO_x formation with the larger-diameter nozzle [36]. The performance and emission characteristics of diesel engines powered by renewable fuels using an experimental ANN technique has been reported in the literature. A comprehensive review on the thermochemical conversion of waste biomass to biofuels has also been presented in the literature.

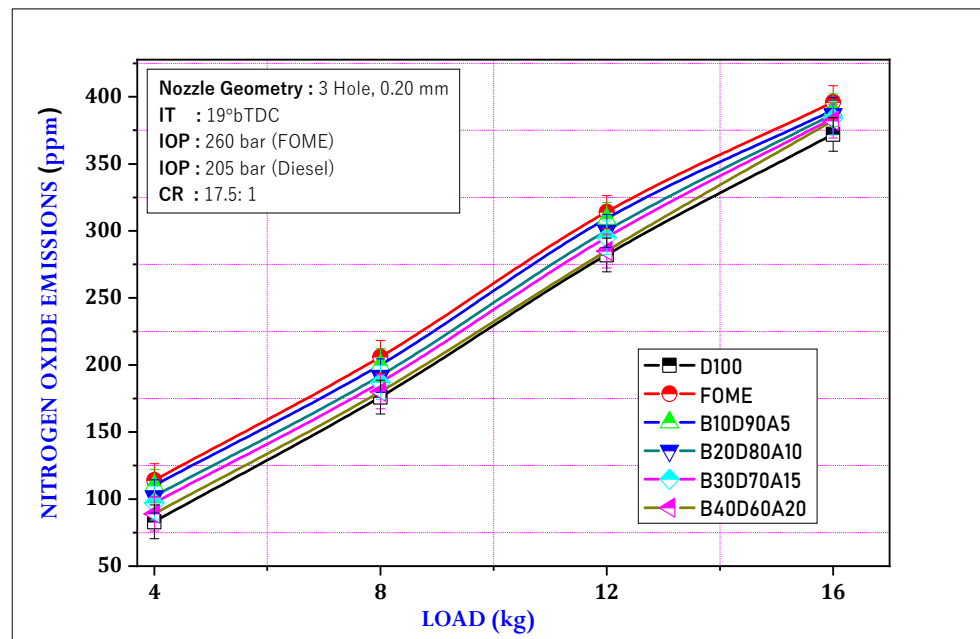


(a)

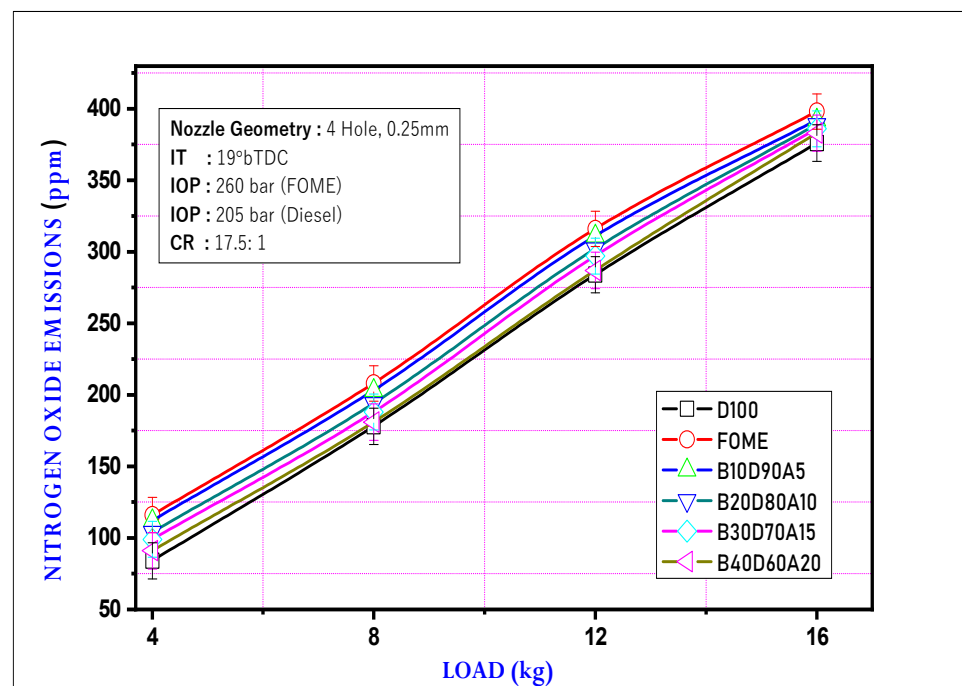


(b)

Figure 10. (a) Variation in HC emission with load for the 3-hole fuel injector. (b) Variation in HC emission with load for the 4-hole fuel injector.



(a)



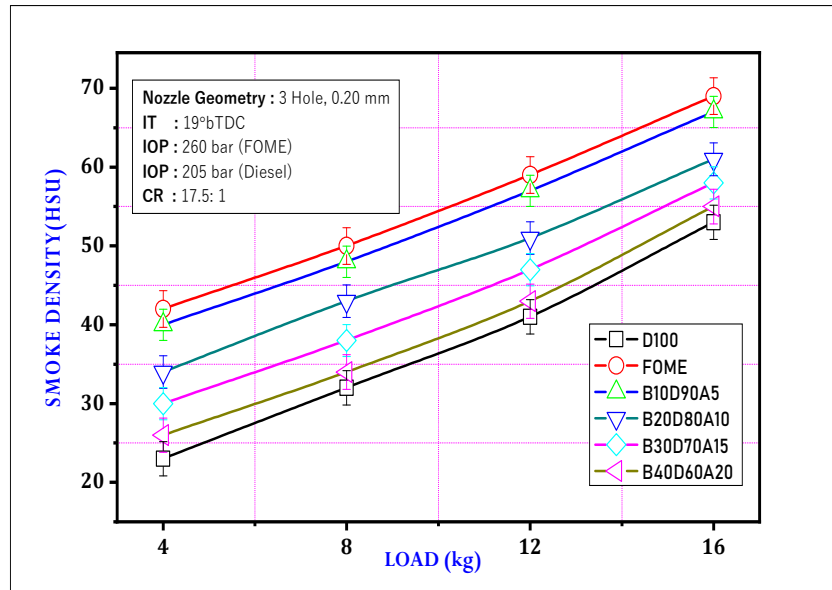
(b)

Figure 11. (a) Variation in NO_x emission with load for the 3-hole fuel injector. (b) Variation in NO_x emission with load for the 4-hole fuel injector.

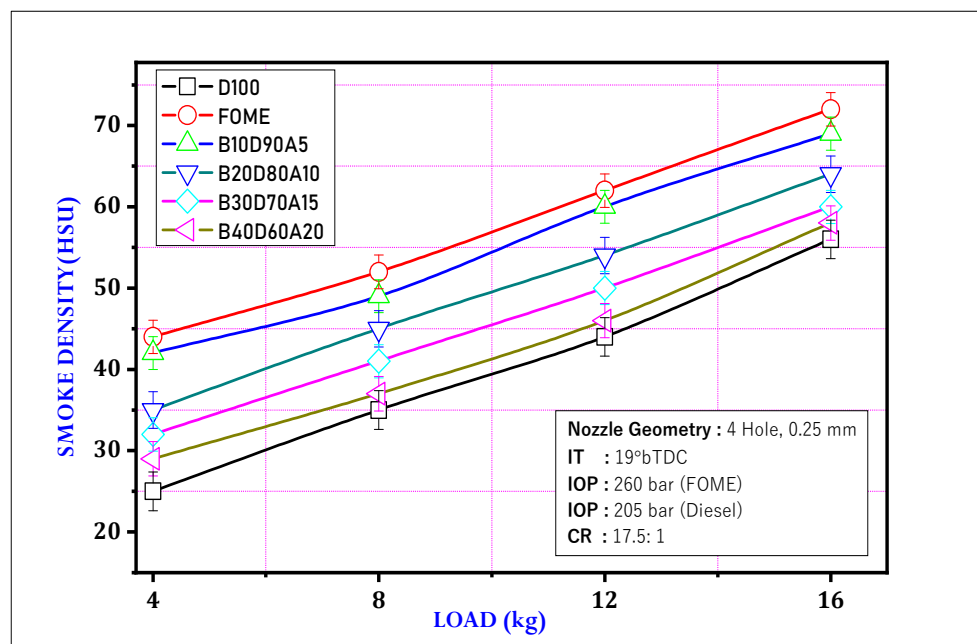
4.6. Emission Comparison—Smoke Opacity

Figure 12a,b illustrate the variation in smoke opacity with load for the blends of diesel, FOME, and Al_2O_3 nanoparticles at three-hole and four-hole nozzle geometries, respectively. In comparison, the biodiesel fuel shows more smoke opacity than diesel fuel. After blending nanoparticles into the biodiesel, the smoke opacity is reduced. The main reason behind this is the large asymmetric surface area and larger thermal conductivity

of nanoparticles [51]. Al₂O₃ nanoparticles transmit enough heat to combustion particles, thereby increasing the oxidation of carbon particles, causing a noteworthy reduction in smoke. There is an increase in smoke emissions at maximum loads as a greater amount of smoke enters the combustion chamber. From the graph, it is evident that out of all the test blends, blend B40D60A20 indicated optimised smoke opacity values that are 3.77% inferior to those of diesel fuel and 20.89% inferior to those of FOME biodiesel with a three-hole nozzle geometry. The blend B40D60A20 also indicated similar trends for the four-hole nozzle geometry, where the smoke opacity values were 3.57% inferior to those of diesel fuel and 20% inferior to those of FOME biodiesel [36].



(a)



(b)

Figure 12. (a) Variation in smoke emission with load for 3-hole fuel injector. (b) Variation in smoke emission with load for 4-hole fuel injector.

4.7. Combustion Characteristics: In-Cylinder Pressure and Heat Release Rate

The calorific value and combustion properties of fuel have a considerable impact on its HRR. Combustion dynamics are broadly classified as pre-mixed combustion and diffusive cycle combustion [55]. Figure 13 shows the variation in the in-cylinder pressure at a crank angle of 100% load using a four-hole fuel injector for nano-biodiesel blends with varied dosages of nanoparticles. Figure 14 demonstrates the variance in the HRR with the CA at maximum load when using a four-hole FI for nano-BD blends with varying nanoparticle doses. The HRR was calculated using a 1-d thermodynamics model and integrated pressures for 100 cycles. Higher doses of nanoparticles in biodiesel and their blends resulted in a higher HRR because these blends improved peak in-cylinder pressures with an enhanced pre-mixed combustion phase and a higher BTE. The heat release for each blend may be calculated from Equation (3). The blend B40D60A20 presented the highest HRR of 80.55 J/degrees and in-cylinder pressure followed by B30D70A15 because of the oxygen present in the Al_2O_3 NPs and high cetane number, which allow for several ignition centres to be generated at different points within the combustion chamber, increasing the rate of combustion at the premixed zone.

$$\left(\frac{dQ_n}{d\theta}\right) = \left(\frac{\gamma}{\gamma-1} P \frac{dV}{d\theta}\right) + \left(\frac{1}{\gamma-1} V \frac{dP}{d\theta}\right) + Q_{lw} \quad (3)$$

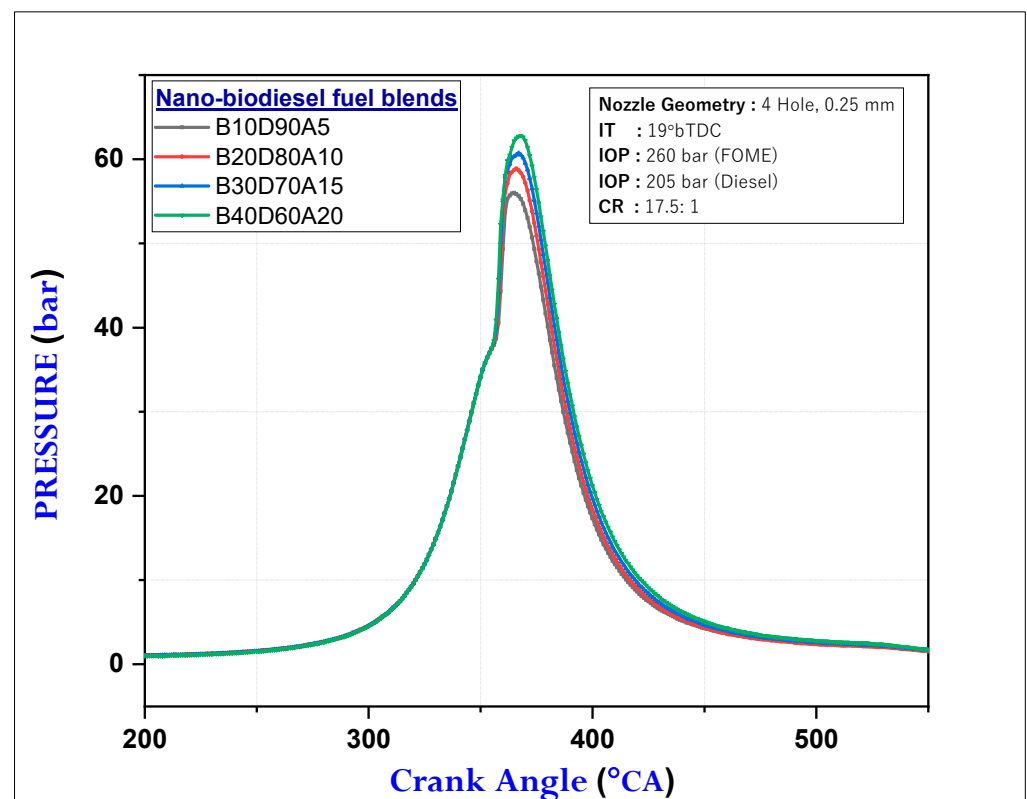


Figure 13. Variation in in-cylinder pressure with crank angle at 100% load.

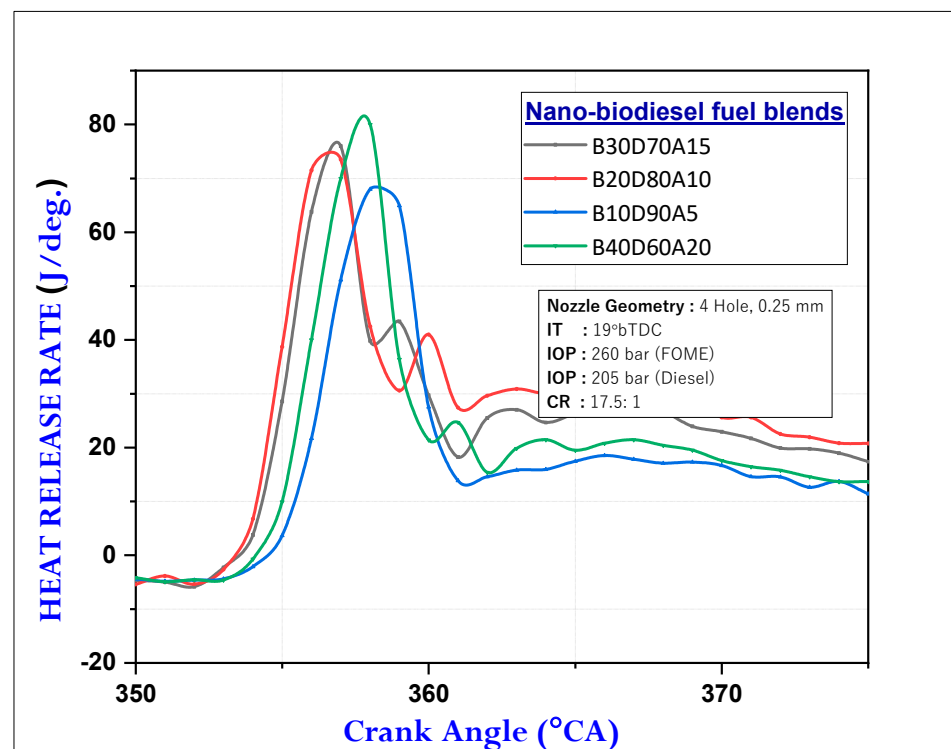


Figure 14. Variation in heat release rate with crank angle at 100% load.

5. Conclusions

The present experimental work was conducted in order to analyse the emissions and performance characteristics of a CI engine fuelled by a mixture of diesel–FOME biodiesel fuel blends with aluminium nanoparticles at varying concentrations—5, 10, 15, and 20 ppm—in the fuel blend. The conclusions of this experimental work are summarised as follows.

1. The B40D60A20 mixture exhibited optimised results for a three-hole nozzle geometry with a 0.20mm orifice diameter and 260 bar pressure injection, wherein a reasonable increase in the BTE and reduced emissions were achieved.
2. Due to the catalytic character of Al_2O_3 , the addition of Al_2O_3 nanoparticles at 20 mg/L in the FOME mixtures, i.e., the B40D60A20 mixture, provided the highest thermal efficiency of 30.9%, which is about 15.53% greater than the 100% FOME and 3.43% lower than the diesel, and also revealed a decrease in CO of 45.46%, HC of 17.29% 5%, NO_x , and smoke of 21.28% compared to raw FOME. Additionally, the emissions are comparable with diesel at all loads.
3. Owing to the uneven nozzle geometry of the four-hole injector, there is a lower BTE and more emissions for the four-hole injector compared to the three-hole injector. As the nozzle diameter decreases, the injection pattern improves, resulting in an enhancement in the engine performance and emission parameters.
4. While the engine operated with a larger-diameter nozzle, the NO_x emissions were lower than those of the smaller diameter nozzle. The cause for this might be attributed to the deterioration of the injection parameter, resulting in the deterioration of the combustion course. With the deterioration of the combustion course, the fuel is not properly burned and the temperature in the cylinder does not increase. Thus, the NO_x emissions were lower for the larger-diameter nozzle.
5. A small-diameter nozzle achieves superior atomization by forming smaller-diameter fuel droplets, thereby enabling an improved air/fuel ratio and facilitating the combustion process. Therefore, a small-diameter injector leads to improved performance and emissions characteristics.

6. Al_2O_3 potentiates an oxygen surge and further oxidises the unburned fuel inside the combustion cavity. As a result of the existence of Al_2O_3 in the test fuel, the levels of imperfect combustion products such as HC, CO, and smoke are significantly lowered for the B40D60A20 mixture.

Author Contributions: Conceptualization, M.E.M.S.; Methodology, S.N.T., A.R.B. and A.M.G.; Software, M.E.M.S., T.M.Y.K. and A.M.G.; Validation, S.N.T., I.V. and M.M.S.; Formal analysis, K.M.A., N.R.B., M.E.M.S., A.S.E.-S. and M.A.K.; Investigation, K.M.A., S.C.K., A.R.B. and M.M.S.; Resources, K.M.A.; Data curation, K.M.A. and A.R.B.; Writing—original draft, T.M.Y.K. and A.S.E.-S.; Writing—review & editing, I.V.; Supervision, M.A.K.; Project administration, N.R.B. and A.S.E.-S.; Funding acquisition, T.M.Y.K. All authors have read and agreed to the published version of the manuscript.

Funding: This work was funded by King Khalid University under grant number R.G.P. 1/214/43.

Data Availability Statement: The data presented in this study are available upon request from the first corresponding author.

Acknowledgments: The authors extend their appreciation to the Deanship of Scientific Research at King Khalid University for funding this work through the research groups program R.G.P. 1/214/43.

Conflicts of Interest: The authors declare no conflict of interest.

Future Scope of Work: In the context of the scope of the present work, further higher performance and lower emissions can be obtained by replacing this single-cylinder engine with a Common Rail Direct Injection (CRDI) engine because it has a 1000 bar to 3000 bar injection pressure and is inhibited by an Electronic Control Unit (ECU). Future studies can explore the properties of diesel engines with various combustion geometries, and the use of ANN and Taguchi techniques to optimise CI engine parameters.

Abbreviations

FOME	Fish Oil Methyl Ester
CI	Compression Ignition
BP	Brake Power
BSFC	Brake Specific Fuel Consumption
HC	Hydrocarbons
CO	Carbon Monoxide
CO_2	Carbon Dioxide
CV	Calorific Value
NO	Nitrous Oxide
NO_x	Nitrogen Oxide
CRDI	Common Rail Direct Injection
CR	Compression Ratio
CNT	Carbon Nanotubes
BTE	Brake Thermal Efficiency
BSFC	Brake Specific Fuel Consumption
UHC	Unburnt Hydrocarbon
JBD	Jatropha Biodiesel
FFA	Free Fatty Acid
HCS	Hexagonal Crystal Structure
B10/B20	FOME 10% + Diesel 90%/ FOME 20% + Diesel 80%/
B30/B40	FOME 30% + Diesel 70%/ FOME 40% + Diesel 60%/
B10D90A5	B10 + 5 ppm Al_2O_3 nanoparticles
B20D80A10	B20 + 10 ppm Al_2O_3 nanoparticles
B30D70A15	B10 + 15 ppm Al_2O_3 nanoparticles
B40D60A20	B10 + 20 ppm Al_2O_3 nanoparticles

References

1. Sarıdemir, S.; Ağbulut, Ü. Combustion, performance, vibration and noise characteristics of cottonseed methyl ester–diesel blends fuelled engine. *Biofuels* **2019**, *13*, 201–210. [[CrossRef](#)]
2. Ağbulut, Ü.; Elibol, E.; Demirci, T.; Sarıdemir, S.; Gürel, A.E.; Rajak, U.; Afzal, A.; Verma, T.N. Synthesis of graphene oxide nanoparticles and the influences of their usage as fuel additives on CI engine behaviors. *Energy* **2021**, *244*, 122603. [[CrossRef](#)]
3. Sharma, P.; Sahoo, B.B. Precise prediction of performance and emission of a waste derived Biogas–Biodiesel powered Dual–Fuel engine using modern ensemble Boosted regression Tree: A critique to Artificial neural network. *Fuel* **2022**, *321*, 124131. [[CrossRef](#)]
4. Bora, B.J.; Saha, U.K. Emission reduction operating parameters for a dual-fuel diesel engine run on biogas and rice-bran biodiesel. *J. Energy Eng.* **2017**, *143*, 04016064. [[CrossRef](#)]
5. Rajak, U.; Ağbulut, Ü.; Veza, I.; Dasore, A.; Sarıdemir, S.; Verma, T.N. Numerical and experimental investigation of a CI engine behaviours supported by zinc oxide nanomaterial along with diesel fuel. *Energy* **2021**, *239*, 122424. [[CrossRef](#)]
6. Ağbulut, Ü.; Karagöz, M.; Sarıdemir, S.; Öztürk, A. Impact of various metal-oxide based nanoparticles and biodiesel blends on the combustion, performance, emission, vibration and noise characteristics of a CI engine. *Fuel* **2020**, *270*, 117521. [[CrossRef](#)]
7. Jha, S.; Nanda, S.; Acharya, B.; Dalai, A.K. A Review of Thermochemical Conversion of Waste Biomass to Biofuels. *Energies* **2022**, *15*, 6352. [[CrossRef](#)]
8. Ağbulut, Ü.; Sarıdemir, S.; Karagöz, M. Experimental investigation of fusel oil (isoamyl alcohol) and diesel blends in a CI engine. *Fuel* **2020**, *267*, 117042. [[CrossRef](#)]
9. Gürbüz, H.; Akçay, H.; Aldemir, M.; Akçay, I.H.; Topalçı, Ü. The effect of euro diesel-hydrogen dual fuel combustion on performance and environmental-economic indicators in a small UAV turbojet engine. *Fuel* **2021**, *306*, 121735. [[CrossRef](#)]
10. Karagöz, M.; Ağbulut, Ü.; Sarıdemir, S. Waste to energy: Production of waste tire pyrolysis oil and comprehensive analysis of its usability in diesel engines. *Fuel* **2020**, *275*, 117844. [[CrossRef](#)]
11. Jabbr, A.I.; Gaja, H.; Koşlu, U.O. Multi-objective optimization of operating parameters for a H₂/Diesel dual-fuel compression-ignition engine. *Int. J. Hydrog. Energy* **2020**, *45*, 19965–19975. [[CrossRef](#)]
12. Ağbulut, Ü.; Sarıdemir, S.; Albayrak, S. Experimental investigation of combustion, performance and emission characteristics of a diesel engine fuelled with diesel–biodiesel–alcohol blends. *J. Braz. Soc. Mech. Sci. Eng.* **2019**, *41*, 1–12. [[CrossRef](#)]
13. Kannan, B.T.; Sathish, T.; Sathyamurthy, R.; Erko, K.G. Use of waste fish oil biodiesel blended with aluminium oxide nanoparticle in IC engines: An experimental on performance, combustion and emission study. *Sci. Rep.* **2022**, *12*, 12930. [[CrossRef](#)]
14. Attia, A.M.A.; El-Seesy, A.I.; El-Batsh, H.M.; Shehata, M.S. Effects of Alumina Nanoparticles Additives into Jojoba Methyl Ester–Diesel Mixture on Diesel Engine Performance. In Proceedings of the ASME International Mechanical Engineering Congress and Exposition, Montreal, QC, Canada, 14–20 November 2014; American Society of Mechanical Engineers: New York, NY, USA, 2014.
15. El-Seesy, A.I.; Abdel-Rahman, A.K.; Bady, M.; Ookawara, S. The influence of multi-walled carbon nanotubes additives into non-edible biodiesel–diesel fuel blend on diesel engine performance and emissions. *Energy Procedia* **2016**, *100*, 166–172. [[CrossRef](#)]
16. Selvan, V.A.M.; Anand, R.; Udayakumar, M. Effects of cerium oxide nanoparticle addition in diesel and diesel–biodiesel–ethanol blends on the performance and emission characteristics of a CI engine. *J. Eng. Appl. Sci.* **2009**, *4*, 1819–6608.
17. Jerryraj Kumar, L.; Anbarasu, G.; Elangovan, T. Effects on nano additives on performance and emission characteristics of calophyllum inophyllum biodiesel. *Int. J. ChemTech Res.* **2016**, *9*, 210–219.
18. Karthikeyan, S.; Elango, A.; Silaimani, S.M.; Prathima, A. Role of Al₂O₃ nano additive in GSOBiodiesel on the working characteristics of a CI engine. *Indian J. Chem. Technol.* **2014**, *21*, 285–289.
19. Jayanthi, P.; Rao, M.S. Effects of nanoparticles additives on performance and emissions characteristics of a DI diesel engine fuelled with biodiesel. *Int. J. Adv. Eng. Technol.* **2016**, *9*, 689.
20. Loganathan, C.S. Emission Reduction from A Diesel Engine Fueled By Cerium Oxide Nano-Additives Using Scr With Different Metal Oxides Coated Catalytic Converter. *J. Eng. Sci. Technol.* **2015**, *10*, 1404–1421.
21. Sravani, K.; Ravindra Reddy, G. Performance and emission characteristics of CI engine when fuelled with Pongamia biodiesel and zinc oxide nano fluid as additive. *Int. J. Eng. Res.* **2016**, *5*, 684–687.
22. Karthikeyan, S.; Elango, A.; Prathima, A. Diesel engine performance and emission analysis using canola oil methyl ester with the nano sized zinc oxide particles. *Indian J. Eng. Mater. Sci.* **2014**, *21*, 83–87.
23. Mohan, N.; Sharma, M.; Singh, R.C.; Pandey, R.K. Performance study of diesel engine using nanofuel. *Int. J. Adv. Res. Innov.* **2015**, *3*, 665–668.
24. Raj, N.M.; Gajendiran, M.; Pitchandi, K.; Nallusamy, N. Investigation on aluminium oxide nano particles blended diesel fuel combustion, performance and emission characteristics of a diesel engine. *J. Chem. Pharm. Res.* **2016**, *8*, 246–257.
25. Prabhu, L.; Kumar, S.S.; Anderson, A.; Rajan, K. Investigation on performance and emission analysis of TiO₂ nanoparticle as an additive for biodiesel blends. *J. Chem. Pharm. Sci. Spec.* **2015**, *7*, 408–412.
26. Ghogare, P.; Kale, N. Experimental investigation on single cylinder diesel engine fuelled with soya bean biodiesel blends with nano additives. *Int. J. Pure Appl. Res. Eng. Technol.* **2016**, *4*, 247–257.
27. Arockiasamy, P.; Anand, R.B. Performance, combustion and emission characteristics of a DI diesel engine fuelled with nanoparticle blended jatropha biodiesel. *Period. Polytech. Mech. Eng.* **2015**, *59*, 88–93. [[CrossRef](#)]
28. Raja, M.; Vijayan, R.; Suresh, S.; Vivekananthan, R. Effect of heat transfer enhancement and NO_x emission using Al₂O₃/water nanofluid as coolant in CI engine. *Indian J. Eng. Mater. Sci.* **2013**, *20*, 443–449.

29. Ramarao, K.; Rao, C.; Sreeramulu, D. The experimental investigation on performance and emission characteristics of a single cylinder diesel engine using nano additives in diesel and biodiesel. *Indian J. Sci. Technol.* **2015**, *8*, 1. [[CrossRef](#)]
30. Saifuddin, M.; Boyce, A.N. Biodiesel Production from Fish (*Cyprinus carpio*) Waste and Evaluation of Engine Performance. *Sains Malays.* **2017**, *46*, 1771–1778. [[CrossRef](#)]
31. Edgar, S. Alumina (Al₂O₃) Nanoparticles—Properties & Applications. In *AZO Nano*; AZO Nano: Manchester, UK, 2013.
32. Basha, J.S.; Anand, R. Performance, emission and combustion characteristics of a diesel engine using Carbon Nanotubes blended Jatropa Methyl Ester Emulsions. *Alex. Eng. J.* **2014**, *53*, 259–273. [[CrossRef](#)]
33. Anbarsooz, M. Combustion characteristics of nanofuels: A comprehensive review on diesel/biodiesel-based nanofuels. *Fuel* **2022**, 126834. [[CrossRef](#)]
34. Ahmed, S.A.; Soudagar, M.E.M.; Rahamathullah, I.; Basha, J.S.; Khan, T.Y.; Javed, S.; Elfakhany, A.; Kalam, M. Investigation of ternary blends of animal fat biodiesel-diethyl ether-diesel fuel on CMFIS-CI engine characteristics. *Fuel* **2023**, *332*, 126200. [[CrossRef](#)]
35. Kattimani, S.S.; Topannavar, S.; Shivashimpi, M.; Dodamani, B. Experimental investigation to optimize fuel injection strategies and compression ratio on single cylinder DI diesel engine operated with FOME biodiesel. *Energy* **2020**, *200*, 117336. [[CrossRef](#)]
36. Kothiwale, G.R.; Akkoli, K.M.; Doddamani, B.M.; Kattimani, S.S.; Ağbulut, U.; Afzal, A.; Kaladgi, A.R.; Said, Z. Impact of injector nozzle diameter and hole number on performance and emission characteristics of CI engine powered by nanoparticles. *Int. J. Environ. Sci. Technol.* **2022**, 1–22. [[CrossRef](#)]
37. Gavhane, R.S.; Kate, A.M.; Pawar, A.; Safaei, M.R.; Soudagar, M.E.; Mujtaba Abbas, M.; Muhammad Ali, H.; Banapurmath, N.R.; Goodarzi, M.; Badruddin, I.A.; et al. Effect of zinc oxide nano-additives and soybean biodiesel at varying loads and compression ratios on VCR diesel engine characteristics. *Symmetry* **2020**, *12*, 1042. [[CrossRef](#)]
38. Soudagar, M.E.M.; Mujtaba, M.A.; Safaei, M.R.; Afzal, A.; Ahmed, W.; Banapurmath, N.R.; Hossain, N.; Bashir, S.; Badruddin, I.A.; Goodarzi, M.; et al. Effect of Sr@ ZnO nanoparticles and Ricinus communis biodiesel-diesel fuel blends on modified CRDI diesel engine characteristics. *Energy* **2021**, *215*, 119094. [[CrossRef](#)]
39. Ağbulut, Ü.; Polat, F.; Sarıdemir, S. A comprehensive study on the influences of different types of nano-sized particles usage in diesel-bioethanol blends on combustion, performance, and environmental aspects. *Energy* **2021**, *229*, 120548. [[CrossRef](#)]
40. Raju, V.D.; Kishore, P.S.; Nanthagopal, K.; Ashok, B. An experimental study on the effect of nanoparticles with novel tamarind seed methyl ester for diesel engine applications. *Energy Convers. Manag.* **2018**, *164*, 655–666. [[CrossRef](#)]
41. El-Seesy, A.I.; Abdel-Rahman, A.K.; Bady, M.; Ookawara, S. Performance, combustion, and emission characteristics of a diesel engine fueled by biodiesel-diesel mixtures with multi-walled carbon nanotubes additives. *Energy Convers. Manag.* **2017**, *135*, 373–393. [[CrossRef](#)]
42. Wei, J.; He, C.; Lv, G.; Zhuang, Y.; Qian, Y.; Pan, S. The combustion, performance and emissions investigation of a dual-fuel diesel engine using silicon dioxide nanoparticle additives to methanol. *Energy* **2021**, *230*, 120734. [[CrossRef](#)]
43. Muruganatham, P.; Pandiyan, P.; Sathyamurthy, R. Analysis on performance and emission characteristics of corn oil methyl ester blended with diesel and cerium oxide nanoparticle. *Case Stud. Therm. Eng.* **2021**, *26*, 101077.
44. Al-Kheraif, A.A.; Syed, A.; Elgorban, A.M.; Divakar, D.D.; Shanmuganathan, R.; Brindhadevi, K. Experimental assessment of performance, combustion and emission characteristics of diesel engine fuelled by combined non-edible blends with nanoparticles. *Fuel* **2021**, *295*, 120590. [[CrossRef](#)]
45. Rastogi, P.M.; Sharma, A.; Kumar, N. Effect of CuO nanoparticles concentration on the performance and emission characteristics of the diesel engine running on jojoba (*Simmondsia Chinensis*) biodiesel. *Fuel* **2021**, *286*, 119358. [[CrossRef](#)]
46. Sivakumar, M.; Sundaram, N.S.; Kumar, R.R.; Thasthagir, M.H.S. Effect of aluminium oxide nanoparticles blended pongamia methyl ester on performance, combustion and emission characteristics of diesel engine. *Renew. Energy* **2018**, *116*, 518–526. [[CrossRef](#)]
47. Hoseini, S.; Najafi, G.; Ghobadian, B.; Mamat, R.; Ebadi, M.; Yusaf, T. Novel environmentally friendly fuel: The effects of nanographene oxide additives on the performance and emission characteristics of diesel engines fuelled with Ailanthus altissima biodiesel. *Renew. Energy* **2018**, *125*, 283–294. [[CrossRef](#)]
48. Hoseini, S.S.; Najafi, G.; Ghobadian, B.; Ebadi, M.T.; Mamat, R.; Yusaf, T. Performance and emission characteristics of a CI engine using graphene oxide (GO) nano-particles additives in biodiesel-diesel blends. *Renew. Energy* **2020**, *145*, 458–465. [[CrossRef](#)]
49. Vigneswaran, R.; Balasubramanian, D.; Sastha, B.S. Performance, emission and combustion characteristics of unmodified diesel engine with titanium dioxide (TiO₂) nano particle along with water-in-diesel emulsion fuel. *Fuel* **2021**, *285*, 119115. [[CrossRef](#)]
50. Singh, V.K.; Ansari, N.A.; Arora, A. A review of ci engine performance and emissions with graphene nanoparticle additive in diesel and biodiesel blends. *Adv. Manuf. Ind. Eng.* **2021**, 1065–1072. [[CrossRef](#)]
51. Annamalai, M.; Dhinesh, B.; Nanthagopal, K.; SivaramaKrishnan, P.; Lalvani, J.I.J.; Parthasarathy, M. An assessment on performance, combustion and emission behavior of a diesel engine powered by ceria nanoparticle blended emulsified biofuel. *Energy Convers. Manag.* **2016**, *123*, 372–380. [[CrossRef](#)]
52. Leach, F.C.; Davy, M.; Terry, B. Combustion and emissions from cerium oxide nanoparticle dosed diesel fuel in a high speed diesel research engine under low temperature combustion (LTC) conditions. *Fuel* **2021**, *288*, 119636. [[CrossRef](#)]
53. Sarıdemir, S.; Yildiz, G.; Hanedar, E. Effect of diesel-biodiesel-methanol blends on performance and combustion characteristics of diesel engine. *Düzce Üniversitesi Bilim Teknol. Derg.* **2021**, *9*, 189–201. [[CrossRef](#)]

-
54. Şen, M.; Emiroglu, A.O.; Keskin, A. Impact of pentanol addition and injection timing on the characteristics of a single-cylinder diesel engine. *Energy Fuels* **2019**, *33*, 9224–9231. [[CrossRef](#)]
 55. Jahanbakhshi, A.; Karami-Boozhani, S.; Yousefi, M.; Ooi, J.B. Performance of bioethanol and diesel fuel by thermodynamic simulation of the miller cycle in the diesel engine. *Results Eng.* **2021**, *12*, 100279. [[CrossRef](#)]